

Physiological significance of TRPV4 channels in  
mouse Schwann cells

Feng Xiaona

Doctor of Philosophy  
(Science)

Department of Physiological Sciences,  
School of Life Science  
The Graduate University for Advanced Studies  
2019

## Index

1. Abstract .....	2
2. Introduction.....	4
3. Materials and Methods .....	8
4. Results .....	15
4.1 TRPV4 is functionally expressed in cultured mouse Schwann cells. ....	15
4.2 Myelin structural proteins, P0, MBP and MAG, are similarly expressed in WT and TRPV4KO mice during normal myelin development. ....	16
4.3 TRPV4 is increased in Schwann cells after sciatic nerve injury. ....	17
4.4 Increased TRPV4 after sciatic nerve injury is attributed to increased unmyelinating Schwann cells. ....	18
4.5 TRPV4 is activated under physiological conditions. ....	18
4.6 TRPV4KO mice show increased levels of P0, MAG and MBP protein after sciatic nerve injury compared with WT mice. ....	19
4.7 Remyelination and functional recovery of sciatic nerves is delayed after sciatic nerve injury in TRPV4KO mice compared with WT mice. ....	19
5. Discussion.....	21
6. Acknowledgments.....	25
7. References.....	26
8. Figure Legends.....	34
9. Tables and Figures .....	40

## 1. Abstract

Schwann cells (SCs) are the primary glial cells of the peripheral nervous system. Myelinating SCs wrap around large-diameter axons and form the myelin sheath. While many transcription factors and signaling molecules are involved in SC myelination, calcium signaling has been found to be an important mediator of this process. Transient receptor potential vanilloid 4 (TRPV4), a member of the TRP channel family, is a non-selective calcium ( $\text{Ca}^{2+}$ )-permeable cation channel. TRPV4 is expressed and activated throughout the body by various stimuli including mechanical stimulation, moderate heat, osmolarity and some endogenous or exogenous chemicals. According to recent reports, this channel was found to be widely expressed and functional in various glial cells, including astrocytes, microglia, oligodendrocytes and satellite glial cells. However, whether TRPV4 is expressed and functional in SCs or not remains unclear. To clarify the expression and function of TRPV4 in SCs, I isolated and purified SCs from the sciatic nerves of postnatal and adult mice. RT-PCR and western blot analyses suggested that TRPV4 is expressed in cultured SCs. Functional expression of TRPV4 was confirmed using calcium-imaging and whole-cell patch-clamp methods. In addition, TRPV4 was found to be expressed in sciatic nerves *in vivo* by western blot. However, there was no clear difference in the expression of the key myelin structural proteins such as myelin-associated glycoprotein (MAG), myelin protein zero (PO) and myelin basic protein (MBP) between WT and TRPV4KO mice, suggesting that TRPV4 is not involved in normal myelin development in mice. However, after sciatic nerve cut injury, TRPV4 expression gradually increased with sciatic nerve demyelination, even under conditions without macrophages which are known to express TRPV4. This suggests that the increase in TRPV4 after sciatic nerve injury is mainly derived from SCs. Furthermore, I confirmed that TRPV4 is expressed in unmyelinating SCs, but not in myelinating SCs, and that unmyelinating SCs were increased after nerve injury. These results suggest why TRPV4 was increased after injury. In addition, TRPV4-dependent intracellular calcium increases were clearly observed in the unmyelinating SCs under body temperature. Interestingly, the lack of TRPV4 resulted in a large amount of myelin protein accumulation at the injury sites, which impaired sciatic nerve functional recovery at 2 months after injury. Electron microscopy showed thinner myelin sheaths in TRPV4KO mice than WT at 2 months after sciatic nerve injury.

However, the sciatic nerve function and the remyelination were similarly recovered by 6 months both in between WT and TRPV4KO mice after injury. In conclusion, TRPV4 is functionally expressed in mouse SCs and is involved in remyelination after sciatic nerve cut injury.

## 2. Introduction

The myelin sheath is a multi-lamellar, lipid-rich structure that wraps large-diameter axons in the vertebrate nervous system. It can be divided into two domains, compact and non-compact myelin, each containing a non-overlapping set of proteins with specialized functions. For example, myelin protein zero (P0), myelin basic protein (MBP) and peripheral myelin protein 22 (PMP22) are localized to compact myelin and function as the main myelin structural proteins (1). In contrast, myelin-associated glycoprotein (MAG) is localized to non-compact myelin and is required for myelin and axonal maintenance (2). Intact myelin provides support and insulation to the axon, which is essential to achieve rapid saltatory impulse conduction. The formation of the myelin sheath is carried out exclusively by two specialized types of glial cells, oligodendrocytes in the central nervous system (CNS) and Schwann cells (SCs) in the peripheral nervous system (PNS). A single oligodendrocyte can extend its processes to myelinate multiple axonal segments, while one SC wraps around only a single axon with its whole body (3).

SCs originate from SC precursors, which in turn arise from multi-potent neural crest cells that delaminate from the dorsal neural tube (4). Around embryonic days 15-16 (E15-E16) in mice, SC precursors differentiate into immature SCs (5, 6). Around birth (E19-E20 in mice), axonal sorting and myelination starts in the peripheral nerves. The final destination of immature SCs is subsequently determined by the axons with which the SCs are randomly associated. Immature SCs which contact small-diameter (C fiber) axons differentiate into non-myelinating SCs. When immature SCs are associated with large axons (A $\alpha$ , A $\beta$  or A $\delta$  fiber), the myelination program is selectively activated, and they proceed towards the pro-myelinating phenotype and form mature myelinating SCs with a 1:1 relationship with large-diameter axons. Axonal sorting and myelination in the PNS occur over an extended period during the first three weeks of postnatal life in rodents (7). During development, axonal signals regulate SC proliferation, survival and differentiation. Reciprocally, SCs provide crucial trophic support for developing neurons and profoundly influence axonal properties, especially through myelination (8, 9).

In contrast to the remarkable differentiation process that occurs during development, SCs remain highly plastic in order to maintain axolemmal organization and neuronal health in adulthood (10). Myelin sheath formation is dynamically regulated in response to environmental

stimuli. When peripheral nerves are cut or crushed, the distal stump undergoes Wallerian degeneration. The plasticity of myelinating SCs allows them to respond adaptively to injury and trigger the repair process by cell type conversion (11). Following nerve injury, the distal nerve degenerates while SCs contribute to demyelination. Demyelinating SCs are activated and acquire an immature-like phenotype called “Bünger” or repair SCs, which are essential for nerve repair. Molecules associated with immature-like SCs are up-regulated, including glial fibrillary acidic protein (GFAP), c-Jun, NCAM, and p75<sup>NTR</sup>, whereas myelination-related genes are down-regulated. These include transcription factor Egr2 (Krox20), enzymes of cholesterol synthesis, periaxin, MAG and myelin structural proteins, such as P0 and MBP (12). The demyelinating SCs (repair or Bünger SCs) in the distal stump upregulate some important neurotrophic factors and cell surface proteins, including GDNF, artemin, BDNF, p75<sup>NTR</sup> and N-cadherin which promote neuronal survival and axon growth (13). Meanwhile, the SCs also increase the expression of cytokines including tumor necrosis factor (TNF)- $\alpha$ , interleukin (IL)-1 $\alpha$ , IL-1 $\beta$ , LIF, and MCP-1 which promote macrophage recruitment. Moreover, SCs play a key role in both myelin breakdown and clearance of myelin debris in the PNS. Autophagic processes are activated in SCs (14-17) and cooperate with the recruited macrophages to clear away the distal axon and myelin sheath fragments which potentially inhibit axonal growth (14). At the same time, macrophages secrete additional cytokines to promote vascularization of the distal nerve (18). The demyelinating SCs (repair or Bünger SCs) form tracks that guide regenerating axons back to their targets. Once SC-axon contact is re-established, repair SCs differentiate and remyelinate the regenerated axons, which is necessary for functional recovery of peripheral nerves.

Although there are some differences, a core set of similar transcription factors and signaling molecules are involved in SC differentiation during myelin development and remyelination following injury. Krox20 is a master positive regulator of myelination which promotes transcription of myelin structural proteins and biosynthetic components of myelin lipid synthesis (2, 19-21). Many transcription factors have been implicated in the control of myelination by regulating Krox20 directly or indirectly. For example, Sox10 and Oct6 synergistically induce the expression of Krox20 which contributes to SC myelination, while Sox2 and c-Jun inhibit Krox20 expression which hampers myelination (22, 23). Interestingly, c-Jun is a

negative regulator of myelination during development while it not only suppresses the expression of myelin genes, but also promotes myelinophagy and upregulates some important neurotrophic factors and cell surface proteins to support neuronal survival and axon growth during repair (13). Neuregulin-1 type III (NRG1-III) is another key regulator of myelination which acts by activating ErbB2-ErbB3 receptor complexes in SCs (24). NRG1-III also controls the balance of myelin growth by activation of the PI<sub>3</sub>-kinase/Akt signaling pathway (25). The MEK pathway is also activated by NRG1-III, and MEK-dependent Yy1 phosphorylation is crucial for Krox20 induction and myelination. In addition to these regulators, several other signaling pathways have been compellingly implicated (23, 26), including Notch signaling (27, 28), Raf/Erk signaling (29), PI3K/Akt/mTOR (30, 31) signaling, NF-κB signaling (32, 33), JNK (34) and p38 MAPK signaling(35, 36).

Recently, Ca<sup>2+</sup> signaling has also been found to be an important mediator of SC myelination. Ca<sup>2+</sup> is a second messenger that is regulated by many intracellular pathways in SCs. One such pathway is the calcineurin/nuclear factor of activated T cell (NFAT) pathway which has been shown to be important for Ca<sup>2+</sup> regulation (37, 38). Binding of NRG1-III to ErbB coreceptors activates PLC-γ, resulting in an intracellular Ca<sup>2+</sup> increase followed by dephosphorylation of NFAT and its nuclear translocation. In the nucleus, NFAT forms a complex with Sox10 to activate Krox20 and drive the transcription of P0 (37, 38). In addition, purinergic signaling also plays a critical role in cytosolic Ca<sup>2+</sup>-dependent SC differentiation and myelin formation. ATP released from the axon induces the intracellular Ca<sup>2+</sup> increase in the surrounding SCs via purinergic receptor activation, which is involved in SC differentiation (39) and proper myelin formation (40). Calcium signaling has also been reported to be regulated by Cx32 hemichannel (41) and β-arrestin-mediated signaling (42) during SC proliferation or differentiation. Moreover, local calcium transient activity in myelin sheaths is involved in regulating the distinct stages of myelination in the CNS (43).

Transient receptor potential (TRP) channels are Ca<sup>2+</sup>-permeable non-selective cation channels. In mammals, TRP channels are grouped into six related protein families, TRPC (canonical), TRPV (vanilloid), TRPM (melastatin), TRPA (ankyrin), TRPML (mucolipin) and TRPP (polycystic) (44). TRPA1 is the only member of the TRPA subfamily, found to be expressed in oligodendrocytes. Under ischemic conditions, the increased hydrogen-ion levels in

oligodendrocytes activate the TRPA1 channel causing intracellular  $\text{Ca}^{2+}$  increase and subsequent myelin damage (45). Recently, TRPA1 expression has also been identified in SCs. Activation of TRPA1 by oxidative stress in SCs evokes a  $\text{Ca}^{2+}$ -dependent and NOX1-mediated long-lasting release of  $\text{H}_2\text{O}_2$ , leading to sustained macrophage-dependent neuropathic pain in mice (46).

TRPV4 is a member of the TRPV subfamily. It is activated by various stimuli including mechanical stimulation, moderate heat, osmolarity, some endogenous chemicals such as anandamide, arachidonic acid and its epoxyeicosatrienoic acid metabolites, as well as by a number of exogenous chemical ligands or UVB (47). Previous reports showed that TRPV4 is expressed and activated throughout the body, such as in epithelia, vascular smooth muscle cells and intrapulmonary arteries (48). Interestingly, TRPV4 was recently found to be widely expressed and functional in various glial cells, such as in astrocytes where it plays active roles in regulating neuronal excitability (49). In microglia, TRPV4 is involved in LPS-induced activation (50, 51). In addition, TRPV4 mRNA was shown to be expressed and TRPV4 functioned in the proliferation of oligodendrocyte precursor cells (52). Satellite glial cells, which share the same genesis as SCs, have also been reported to functionally express TRPV4 where it may regulate inflammatory pain by enhancing the purinergic signaling pathway (53). However, there have been no reports of TRPV4 expression in SCs.

In the present thesis, I found that TRPV4 is functionally expressed in mouse SCs and is involved in remyelination after sciatic nerve cut injury. This study is the first report showing the expression and physiological significance of TRPV4 channels in SCs.

### **3. Materials and Methods**

#### ***Mice***

15-week-old C57BL/6NCr male and female mice were used. Mice were kept under a 12-hour light-dark cycle, at 24°C with unlimited food and water. TRPV4-deficient (TRPV4KO) mice were maintained on a C57BL6/NCr background (54). Walking track analysis and electron micrograph experiments were conducted with WT and TRPV4KO male littermates. All animal care and experimental procedures were approved by the institutional Animal Care and Use Committee of the National Institute of Natural Sciences, and performed according to the National Institutes of Health and National Institute for Physiological Sciences guidelines.

#### ***Chemicals***

GSK1016790A (GSK), capsaicin, pregnenolone sulfate (PS), lysophosphatidylcholine (LPC) and ionomycin calcium salt were purchased from Sigma-Aldrich; Allyl isothiocyanate (AITC) was purchased from KANTO; Camphor was purchased from Wake; Fura-2 was purchased from Invitrogen.

#### ***Isolation and purification of mouse Schwann cells (SCs)***

**Isolation of mouse SCs.** Mouse SCs from postnatal day 1-3 (P1-3) mice were established according to a previously reported method (55) with some modifications. Sciatic nerves were isolated, cut into small pieces, and dissociated with 2.5 mg/mL dispase II (D4693, Sigma) and 0.5 mg/mL collagenase type IV (C5138, Sigma) for 30 min. The cells were resuspended in 10 mL of basic growth medium containing DMEM, 10% inactivated horse serum (HS; 26050070, Gibco), 4 mM L-glutamine (25030-081, Sigma), 1% penicillin streptomycin (15140-122, Invitrogen), 2 ng/mL human heregulin- beta 1 (396-HB-050, R&D) and 0.5  $\mu$ M forskolin (F6886, Sigma), and plated into a 100 mm petri dish pre-coated with 100  $\mu$ g/mL poly-L-lysine (P1274, Sigma) and 10 ng/mL laminin (L2020, Sigma) and maintained at 37°C in a 5% CO<sub>2</sub> humidified incubator. Medium was refreshed every two days. Mouse SCs from adult mice were established by modification of previously reported methods (56). Sciatic nerves were isolated from 15-week-old mice, cut into 10 mm segments and explanted into 30 mm dishes containing 750

$\mu$ L high-glucose Dulbecco's modified essential medium (DMEM) with 10% heat-inactivated FBS to facilitate myelin removal and cell recovery (57). Medium was refreshed every two days. Ten days later, nerve explants were dissociated with 2.5 mg/mL dispase II and 0.5 mg/mL collagenase type IV for 30 min. Subsequent steps were identical to those described for postnatal SCs.

**Purification of Schwann cells.** After the SC cultures had reached approximately 80% confluence, contaminating fibroblasts were removed by a complement reaction using Thy 1.1 antibodies (58). Briefly, SCs were washed once with pre-warmed PBS then digested with 0.05% trypsin for 1-2 min. Cell suspensions were collected and washed twice with pre-warmed DMEM/10% HS by centrifugation. The cells were resuspended in 500  $\mu$ L pre-cooled anti-mouse Thy 1.1 antibody (30 ng/ $\mu$ L; MCAO2R, Bio-Rad) in DMEM/10% HS, and incubated on ice for 1 hour to allow antigen and antibody interaction. Antibody solution was removed by centrifugation, then the cell pellet was resuspended in rabbit complement solutions containing 200  $\mu$ L rabbit serum complement (234400, Merck Millipore) with 600  $\mu$ L DMEM medium, and incubated at 37°C for 1 hour. The cell pellet was collected and washed with pre-warmed DMEM by centrifugation. The cells were resuspended in SC growth medium (55) containing basic growth medium, 10 ng/mL human-basic fibroblast growth factor (GF003, Merck Millipore) and 20  $\mu$ g/mL bovine pituitary extract (16500100, Cosmo Bio), and plated into a new dish pre-coated with 100  $\mu$ g/mL poly-L-lysine and 10 ng/mL laminin. The purity of SCs was determined to be greater than 98% by S100 immunostaining. The purified SCs were used in the following experiments.

### ***RT-PCR***

RT-PCR was performed as previously reported (59). Total RNA was isolated from purified primary SCs using Sepasol-RNA I super G (09379-84, Nacalai Tesque). Reverse transcription was performed using Super Script III reverse transcriptase (18080-085, Invitrogen) according to the manufacturer's instructions. RNA concentration and quality were assessed using a Nanodrop (Isogen Life Science, Belgium). To investigate the expression of TRPV4 mRNA, cDNA fragments were amplified using EmeraldAmp MAX PCR Master Mix (DS-RR320A, TaKaRa) with PCR primers designed using pick primers from the National Center for Biotechnology Information (Table 1). All primers spanned an exon-exon junction. The PCR products were confirmed by

electrophoresis on a 2% agarose gel containing ethidium bromide.

### ***Immunostaining***

For immunostaining analysis of cultured SCs, cells were cultured on poly-L-lysine/laminin coated glass coverslips. Cells were washed with PBS and fixed with pre-cooled 4% paraformaldehyde for 10 min and washed in PBS. Cells were incubated with blocking buffer (PBS containing 0.25% Triton X-100 and 1% bovine serum albumin) for 30 min at room temperature (RT), then incubated overnight at 4°C with primary antibody (diluted in blocking buffer). After 3 washes with blocking buffer, secondary antibody (1:1000, diluted in blocking buffer) was applied for 1 h at RT. Cells were then incubated in DAPI solution (D212, Wako) for another 10 min, followed by 3 washes with PBS. Images were obtained with a fluorescence microscope (BZ9000; Keyence, Osaka, Japan).

For immunostaining analysis of sections, mice were perfused with 4% paraformaldehyde. The distal sciatic nerves, which were 1 mm distance from the cut site, were collected and post-fixed in 4% paraformaldehyde at 4°C for 16 h. Fixed sciatic nerves were immersed in 30% sucrose at 4°C for 24 h, then embedded in optimal cutting temperature (OCT) compound, then sectioned at a thickness of 10 µm. Subsequent staining steps were identical to the immunostaining analysis of cultured SCs described above. Images were obtained with a laser-scanning confocal microscope (LSM-510; Carl Zeiss).

For immunostaining analysis of teased sciatic nerves (60), the sciatic nerves were separated without perfusion, and immediately immersed into 4% paraformaldehyde for 1 h at RT. After fixation, the sciatic nerves were washed 3 times in PBS for 10 min each. The sciatic nerves were then transferred onto pre-coated slides, the epineurium and perineurium were removed, and the individual fibers were carefully teased apart using fine forceps under a dissecting microscope. After the teased fibers were dried out, they were directly immersed into prechilled (-20°C) acetone for 20 min at -20°C. Slides were then removed from the acetone and allowed to air dry for 30 s. Subsequent staining steps were identical to the immunostaining analysis of cultured SCs described above. Images were obtained with a fluorescence microscope (BZ9000; Keyence, Osaka, Japan).

The following primary antibodies were used: anti-S100 antibody (1:200; ab868, Abcam),

anti-rabbit Myelin Protein Zero (1:200; ab31851, abcam), anti-rat myelin basic protein (1:200; MAB386, Merk Millipore), anti-mouse MAG (1:300; sc-166848, Santa Cruz Biotechnology), anti-chicken GFAP (1:400; ab4674, Abcam), and anti-rabbit TRPV4 (1:500; CB-ACC-034, Alomone). The following secondary antibodies were used: goat anti-rat IgG Alexa Fluor® 488 (a11006, Invitrogen), goat anti-chicken IgY (H+L) Alexa Fluor® 647 (ab150171, Abcam), goat anti-chicken IgY (H+L) Alexa Fluor® 488 (A11039, Invitrogen), donkey anti-rabbit IgG Alexa Fluor® 488 (A21206, Invitrogen), and goat anti-mouse IgG (H+L) Alexa Fluor® 546 (A11030, Invitrogen).

### ***Western blotting***

Total protein was extracted from purified SCs or sciatic nerves. The purified SCs or sciatic nerves were washed with PBS 3 times, and dissociated in lysis buffer containing 10 mM Tris-HCl, 150 mM NaCl, 1 mM EDTA-2Na, 1% Nonidet P-40, 1 mM Na<sub>2</sub>VO<sub>4</sub>, 10 mM NaF and Protease Inhibitor Cocktail (11873580001, Roche) for 30 min on ice. The supernatants were collected by centrifugation. For western blot of TRPV4, total proteins were used for immunoprecipitation. The supernatants were incubated in a rotator for 2 h with protein-G-coated magnetic beads (GE28-9513-79, GE Healthcare). Following centrifugation, the supernatants were incubated in a rotator for 16 hours with anti-TRPV4 antibody (1:500). Protein-G-coated magnetic beads were added, and incubated in a rotator for 2 h. After incubation, the supernatants were collected and denatured for the loading control (vinculin) detection. And the pellets were washed by lysis buffer, denatured and used for western blot of TRPV4. For other proteins, total protein was denatured and used for western blotting. The following primary antibodies were used in the western blots: anti-rabbit Myelin Protein Zero (ab31851, abcam), anti-rat myelin basic protein (MAB386, Merk Millipore), anti-mouse MAG (sc-166848, Santa Cruz Biotechnology), anti-rabbit TRPV4 (CB-ACC-034, Alomone), anti-rabbit EGR2 (ab108399, abcam), anti-rabbit c-Jun mAb (9165, Cell Signaling Technology), and anti-mouse vinculin antibody (VIN-11-5, Sigma). The following secondary antibodies were used for western blotting: HRP-conjugated GAPDH rabbit mAb (8884, Cell Signaling Technology), HRP-linked anti-rabbit IgG (7074, Cell Signaling Technology), HRP-linked anti-mouse IgG (7076, Cell Signaling Technology), and HRP-linked anti-rat IgG (112-035-062, Jackson).

### ***Calcium imaging***

Purified SCs were cultured on poly-L-lysine/laminin-coated glass coverslips. After loading with 5  $\mu$ M Fura-2-acetoxymethyl ester (Fura-2) for 1 h, SCs were mounted in an open chamber and superfused with bath solution. The standard bath solution contained 140 mM NaCl, 5 mM KCl, 2 mM MgCl<sub>2</sub>, 2 mM CaCl<sub>2</sub>, 10 mM HEPES, 10 mM glucose, and pH 7.4 adjusted with NaOH. For Ca<sup>2+</sup>-free bath solution, 5 mM EGTA was added instead of 2 mM CaCl<sub>2</sub>. All chemicals were dissolved in the standard bath solution. For Ca<sup>2+</sup>-free experiments, chemicals were dissolved in Ca<sup>2+</sup>-free bath solution. All experiments were performed at room temperature unless otherwise stated. For thermal stimulation experiments, SCs were placed at 33°C in a 5% CO<sub>2</sub> humidified incubator 24 h before Fura-2 loading. Thermal stimulation was performed by increasing the bath temperature using pre-warmed standard bath solution (~37°C). The temperature was monitored using a thermocouple (TC-344; Warner Instruments, Hamden, CT, USA) placed into the bath. Cytosolic free Ca<sup>2+</sup> concentrations were measured by dual-wavelength Fura-2 microfluorometry with excitation at 340/380 nm and emission at 510 nm. The ratio image was calculated and acquired using the IP-Lab image processing system (Scanalytics, Milwaukee, WI, USA).

### ***Patch-clamp recording***

Purified SCs were cultured on glass coverslips. Patch pipettes were made from borosilicate glass (type 8250, Garner Glass Company, United States) using a five-step protocol and a P-97 micropipette puller (Sutter Instrument, United States), with a tip resistance of 4 to 6 M $\Omega$ . Currents were recorded using an Axopatch 200B amplifier (Molecular Devices, United States) and filtered at 5 kHz with a low-pass filter. Currents were digitized with Digidata 1440A (Axon Instruments, United States). Data acquisition was achieved with pCLAMP 10 software (Axon Instruments, United States). The standard bath solution was the same as described for the calcium imaging. The cesium chloride pipette solution contained 140 mM CsCl, 5 mM EGTA, 10 mM HEPES, pH 7.40 with CsOH. The holding potential was -60 mV, and the ramp-pulse was from -100 to +100 mV for a 300 ms duration. All data and graphs were statistically analyzed using Origin Pro8 (OriginLab, United States).

### ***Sciatic nerve cut injury***

Sciatic nerve surgeries were performed as reported previously (27). Briefly, mice were anesthetized by isoflurane, the right sciatic nerve was exposed and cut at the sciatic notch (distal stump), then the skin was closed. The distal stumps which were at a 1 mm distance from the cut site were collected for analysis at various time points. Contralateral sciatic nerves were used as controls for immunohistochemistry and electron microscopy analysis. For western blot analysis, either contralateral or uninjured sciatic nerves were used as described in the text.

### ***Sciatic nerve cut injury in vitro***

This experiment was performed by modification of a previously reported method (17). Sciatic nerves from 15-week-old WT and TRPV4KO mice were isolated, cut into 5 mm segments, and seeded onto a 35 mm plate. Nerve segments were cultured in DMEM medium containing 10% FBS and 1% penicillin streptomycin in a 5% CO<sub>2</sub> humidified incubator at 37°C. After 7 days, the cultured nerve segments were collected and total protein was obtained for the western blot analysis of TRPV4.

### ***Walking track analysis***

Walking track analysis was performed as previously reported (61). Mice were placed at the entrance of a corridor (50 cm × 5.5 cm) which contained a darkened carton box at the end. The floor of the corridor was covered with paper tape. The hind paws of mice were painted with ink, and mice walked straight through the corridor into the darkened box, leaving their footprints on the paper. Three legible footprints were selected from the several footprints generated by each mouse, and the sciatic functional index (SFI) value was calculated as previously described (62). Data on paw length (PL) and toe spread (TS) were collected from both the contralateral and ipsilateral hind legs. The value of SFI was calculated using the formula below:

$$\text{Sciatic Functional Index (SFI)} = 118.9 \left( \frac{\text{ETS} - \text{NTS}}{\text{NTS}} \right) - 51.2 \left( \frac{\text{EPL} - \text{NPL}}{\text{NPL}} \right) - 7.5$$

ETS: toe spread (the distance from the first to the fifth toe) of the ipsilateral hind paw; NTS: toe spread of the contralateral hind paw; EPL: paw length (the distance from the heel to the third toe) of the ipsilateral hind paw; NPL: paw length of the contralateral hind paw. In the presence

of a toe contracture, the print length was measured as the paw length plus the length from the proximal knuckle to the end of the toe (63).

### ***Electron microscopy***

Tissue preparation and imaging were performed as previously described (64). The mice used for the walking track analysis were perfused with 2.5% glutaraldehyde and 4% paraformaldehyde in 0.1 M phosphate buffer. The distal sciatic nerves located 1 mm distance from the cut site were collected from WT and TRPV4KO mice, post-fixed for another 4 h, and maintained at 4°C overnight. Samples were treated with 2% OsO<sub>4</sub> in 0.15% potassium ferricyanide for 1 h on ice, followed sequentially by 1% thiocarbohydrazine for 20 min, 2% OsO<sub>4</sub> for 30 min at RT, and 20 μM lead II aspartate solution containing 0.03 M L-aspartic acid solution (pH 5.2-5.5) for 30 min at 60°C. Each of these treatments was followed by washing 5 times with double-distilled water. Then, samples were dehydrated with a graded series of ethanol and acetone respectively, and embedded in 7% carbon conductive resin over 3 days (65). Blocks were trimmed in an ultramicrotome and treated with gold sputtering to increase conductivity. Images were obtained using either field emission-SEM (Merlin or Sigma, Carl Zeiss AG) equipped with 3View (Gatan, Inc.) or transmission electron microscopy (JEM-1400, JEOL Ltd.). Image analysis was performed with Image J software. The g-ratio was calculated based on the diameter of the axon divided by the diameter of the axon including the myelin. The diameter was calculated by the measured perimeter divided by  $\pi$ .

### ***Statistics***

Three independent experiments were performed. Data are presented as the mean  $\pm$  SEM. Statistical analysis was performed with Origin Pro8 (RRID: SCR\_014212; OriginLab, Haverhill, MA, USA). Significant changes were identified using a two-tailed *t*-test, at 95% confidence interval, with  $p < 0.05$  considered as statistically significant ( $p$  values: \*  $< 0.05$ , \*\*  $< 0.01$ ).

## 4. Results

### 4.1 TRPV4 is functionally expressed in cultured mouse Schwann cells.

TRPV4 is widely expressed and has a functional role in various glial cells including astrocytes (49), microglia (50, 51), oligodendrocytes (52) and satellite glial cells (53). However, there is no report of TRPV4 expression in Schwann cells (SCs). To evaluate the expression of TRPV4 in SCs, I isolated and purified SCs from sciatic nerves from postnatal day 1-3 (P1-3) and adult mice. To isolate the adult SCs, I cultured sciatic nerve tissue for 10 days before enzymatic dissociation to facilitate myelin removal (for details see the Materials and Methods). Accordingly, SCs from both P1-3 and adult mice were unmyelinating SCs. Purity of the SCs was confirmed by immunostaining for S100, a marker of SCs, and SC purity was found to be greater than 98% (Fig. 1a). Total mRNA was extracted from the purified SCs. By RT-PCR, I found that TRPV4 mRNA is positively amplified in SCs from both pups and adult mice (Fig. 1b). By western blot analysis, TRPV4 protein was detected in cultured wild-type (WT) SCs, but not in TRPV4-deficient (TRPV4KO) SCs (Fig. 1c). These results indicate that TRPV4 is expressed in cultured SCs.

In addition to this molecular confirmation, further validation of the functional expression of TRPV4 was performed using calcium imaging and whole-cell patch-clamp methods. Calcium imaging experiments showed that a TRPV4 selective agonist, GSK1016790A (GSK, 1.0  $\mu$ M), induced an increase in intracellular  $\text{Ca}^{2+}$  in an extracellular  $\text{Ca}^{2+}$ -dependent manner in cultured WT SCs (Fig. 2a), but not in TRPV4KO SCs (Fig. 2b). This suggests that the intracellular  $\text{Ca}^{2+}$  increase is due to the functional expression of TRPV4 in the plasma membrane, but not from the intracellular  $\text{Ca}^{2+}$  stores. In addition, the TRPV4-mediated responses to GSK were also detected in whole-cell patch-clamp recordings in cultured WT SCs (Fig. 2c). 1.0  $\mu$ M GSK-evoked currents with an outwardly rectifying current-voltage (I-V) relationship were observed (Fig. 2c, inset). Combined, these results demonstrate the endogenous expression of TRPV4 in cultured mouse SCs.

In the meantime, I checked the expression of other TRP channels in the purified SCs. mRNAs of TRPV1, TRPV2, TRPV3, TRPV4 and TRPA1 were positively detected while mRNAs of TRPV5 and TRPM3 were not (Fig. 3a). Functional expression of TRPV1, TRPV2, TRPV3, TRPV4, TRPA1 and TRPM3 was further examined using a calcium imaging method. Capsaicin, allyl

isothiocyanate (AITC), camphor, pregnenolone sulfate (PS) and lysophosphatidylcholine (LPC) are agonists of TRPV1, TRPA1, TRPV3, TRPM3 and TRPV2, respectively. GSK induced a large increase of intracellular  $\text{Ca}^{2+}$  in SCs while LPC induced a small increase. On the other hand, capsaicin, AITC, camphor or PS did not evoke any response. These results suggest that only TRPV2 and TRPV4 are functionally expressed in SCs (Fig. 3b-e). However, the changes in intracellular  $\text{Ca}^{2+}$  concentrations in SCs in response to LPC was subtle and slow even with a very high concentration (30 $\mu\text{M}$ ) (Fig. 3c). In addition, LPC is a nonspecific agonist of TRPV2 and there are no other specific agonists. Accordingly, I decided to focus on the function of TRPV4 in SCs in this study.

#### **4.2 Myelin structural proteins, P0, MBP and MAG, are similarly expressed in WT and TRPV4KO mice during normal myelin development.**

To understand the physiological function of TRPV4 in SCs, I first examined if TRPV4 is involved in normal myelin development in mice. Myelin lamellae are divided into two domains, non-compact and compact myelin. The non-compact myelin participates in SC-axonal or SC-SC interactions whereas compact myelin participates in forming the highly organized myelin lamellae and in electrically insulated axons. MAG is localized to non-compact myelin, which is crucial for myelin and axonal maintenance. In contrast, P0 and MBP are localized to compact myelin, which is a major component of the myelin sheath in peripheral nerves (1, 2). By western blot analysis, I confirmed TRPV4 expression in sciatic nerves from 15-week-old WT mice. However, I did not observe any differences in the expression levels of P0, MBP or MAG in sciatic nerves between 15-week-old WT and TRPV4KO mice (Fig. 4b, Fig. 4c). Neurofilament (NF) 160, an axonal marker, also showed similar expression in WT and TRPV4KO sciatic nerves (Fig. 4c).

Because SC myelination occurs over an extended period during the first three weeks of postnatal life in mice (7), I compared MAG and P0 protein levels in sciatic nerves from WT and TRPV4KO littermates at the following progressive ages: postnatal day 7 (P7; Fig. 5a), postnatal day 15 (P15; Fig. 5b), postnatal day 21 (P21; Fig. 5c) and 8 weeks (Fig. 5d). However, MAG and P0 protein levels were comparable between WT and TRPV4KO littermates. Taken together, these results suggest that TRPV4 is not involved in normal myelin development in mice.

### 4.3 TRPV4 is increased in Schwann cells after sciatic nerve injury.

Next, I investigated whether TRPV4 is involved in pathological conditions. When peripheral nerves are cut or crushed, the distal stumps undergo Wallerian degeneration. This is characterized by the degeneration of the distal nerve followed by SC demyelination. Demyelinating SCs are activated and assume an immature-like SC phenotype (repair SCs) to mediate nerve repair. Meanwhile, autophagy processes are activated in SCs, and they cooperate with recruited macrophages to clear away the fragments of distal axons and myelin sheaths which potentially inhibit axonal growth. Moreover, the demyelinating SCs (repair SCs) form tracks that guide the regenerating axons back to their targets, then distal nerve fibers become remyelinated. SCs are thought to play a key role during this process. To evaluate this further, I created a sciatic nerve cut injury model in mice and examined the role of TRPV4 in this process.

To gain a broader understanding of the processes involved in sciatic nerve cut-induced Wallerian degeneration, I cut the sciatic nerves at the notch region in 15-week-old mice (Fig. 6a). The distal stumps were collected, and protein levels were evaluated from 5 days to 5 weeks after injury. NF160 was completely absent by 5 days after injury, and regeneration was initiated at 14 days after injury. While expression of P0 and MAG began to decrease from the beginning of injury, they reached their lowest levels at 2 weeks after injury, at which point regeneration began (Fig. 6b). Interestingly, TRPV4 gradually increased with sciatic nerve demyelination from 2 to 14 days, and decreased with sciatic nerve remyelination at 21 days (Fig. 6c).

Macrophages, which also express TRPV4, migrate to the distal stump and contribute to debris clearance (Fig. 7a). Given this, I wondered whether the increased TRPV4 protein levels arise from SCs or from macrophages. To answer this question, I performed an *in vitro* experiment of sciatic nerve cut injury (Fig. 7b). In this model, short nerve segments were cultured *in vitro* which causes progressive myelin breakdown, similar to the changes seen *in vivo*. However, in the *in vitro* setting, these processes are mainly performed by SCs because invading macrophages are absent (60). 7 days after injury, short nerve segments underwent Wallerian degeneration, which is consistent with the processes observed *in vivo*. NF160 was mostly absent and MAG was largely decreased. The negative regulator of myelination, c-Jun, was increased, and the positive regulator of myelination, Krox20, was decreased. Importantly, TRPV4 was

clearly increased *in vitro* after injury in WT sciatic nerves (Fig. 7c). These results suggest that the increased TRPV4 in the sciatic nerves after injury is primarily from SCs.

#### **4.4 Increased TRPV4 after sciatic nerve injury is attributed to increased unmyelinating Schwann cells.**

To further understand how TRPV4 protein levels are regulated after injury, the following experiments were performed. I first analyzed the expression pattern of TRPV4 in sciatic nerves from adult WT mice. Sciatic nerves were isolated and individual fibers were carefully teased apart under a dissection microscope, and double immunostaining of TRPV4 with glial fibrillary acidic protein (GFAP) or MBP was performed. GFAP is an intermediate filament III protein expressed by unmyelinating SCs, but not by myelinating SCs (66). I found that TRPV4 is expressed in the GFAP-positive SCs, but not in MBP-positive SCs, indicating that TRPV4 is expressed in unmyelinating SCs from sciatic nerves (Fig. 8). I also confirmed that GFAP is increased in the distal stump 7 days after sciatic nerve injury, indicating an increase in unmyelinating SCs (Fig. 9). Together, these experiments provide evidence that SCs from the distal nerve are gradually demyelinated after sciatic nerve injury, leading to an increase in unmyelinating SCs (Fig. 8), which results in increased TRPV4 protein, since TRPV4 is expressed in unmyelinating SCs.

#### **4.5 TRPV4 is activated under physiological conditions.**

I next examined whether the increased TRPV4 is in an active state under physiological conditions. I measured the temperature-evoked increase in intracellular  $\text{Ca}^{2+}$  using a calcium-imaging method in cultured SCs. Temperature elevation up to 37°C evoked an intracellular  $\text{Ca}^{2+}$  increase; this response was similar to that observed after application of 1  $\mu\text{M}$  GSK in WT SCs (Fig. 10a), but not in TRPV4KO SCs (Fig. 10b). These data indicate that TRPV4 is activated at physiological temperatures, which is consistent with previous reports in other cell types (67, 68).

#### **4.6 TRPV4KO mice show increased levels of P0, MAG and MBP protein after sciatic nerve injury compared with WT mice.**

The above results suggested that TRPV4 expression is increased after sciatic nerve cut injury. I hypothesized that the process of recovery from sciatic nerve cut-induced Wallerian degeneration is affected by the increase in TRPV4 expression. To test this, I created a sciatic nerve cut injury model in both WT and TRPV4KO mice. The time course of P0 and NF160 expression from 7 days to 2 months after injury was evaluated by western blot. After injury, as expected, P0 and NF160 proteins were first decreased, and then increased in both WT and TRPV4KO mice. However, the level of P0 protein was clearly higher in TRPV4KO mice than that of WT mice 1-3 weeks after injury (Fig. 11a). I confirmed this finding by evaluating other myelin structural proteins 7 days after injury. P0, MAG, MBP and NF160 were all decreased after injury, indicating SC demyelination and axon degeneration as described previously (Fig. 6). However, TRPV4KO mice showed significantly higher levels of P0, MAG and MBP proteins in the ipsilateral distal stumps, but not on the contralateral side, when compared with WT mice (Fig. 11b-c).

#### **4.7 Remyelination and functional recovery of sciatic nerves is delayed after sciatic nerve injury in TRPV4KO mice compared with WT mice.**

Changes in myelin structural protein levels during the demyelination process are expected to affect SC remyelination during the recovery stage. Therefore, I examined the phenotype of TRPV4KO mice during the recovery stage after sciatic nerve cut injury. Sciatic nerves were injured in both WT and TRPV4KO mice. Based on the previous results (Fig. 11a), WT and TRPV4KO mice were in the recovery stage by at 2 months after injury. The walking gaits of these mice were compared to assess functional recovery of the injured sciatic nerve. In WT mice, the paws were spread wider than in TRPV4KO mice (Fig. 12a), and most TRPV4KO mice showed severe contracture (4/6) with their toes curled under the paw (Fig. 12a). I quantified the walking gaits by walking track analysis. After applying black ink to their hind paws, mice were allowed to walk through a straight corridor lined with paper tape into a darkened box so they would leave footprints on the paper (Fig. 12b). Print length and toe spread length were measured from the footprint stamps, and sciatic functional index (SFI) values were calculated as previously

described (Fig. 12c) (62, 63). SFI values were significantly smaller in TRPV4KO mice than in WT mice (Fig. 12d;  $-52.7 \pm 3.9$  in WT mice vs.  $-98.3 \pm 2.5$  in TRPV4KO mice;  $p = 0.0002$ ). This indicates that the absence of TRPV4 impairs the functional recovery of sciatic nerves at 2 months after sciatic nerve injury.

To further evaluate the regeneration of sciatic nerves, the structure of the distal stumps from these mice was analyzed using an electron microscope (EM). From the transected nerves, I did not observe any differences in the contralateral sections between WT and TRPV4KO mice (Fig. 13, left). However, the reformed axon diameter in the ipsilateral sections looked thinner compared to the contralateral sides in both genotype groups. Importantly, TRPV4KO mice appeared to have thinner myelin sheaths compared with WT mice (Fig. 13). Accordingly, I evaluated myelin thickness using g-ratio which is calculated as the diameter of the axon divided by the diameter of the axon with myelin included, and found that the g-ratios were significantly larger in TRPV4KO mice than in WT mice (average g-ratios of  $0.677 \pm 0.003$  in WT mice vs.  $0.718 \pm 0.003$  in TRPV4KO mice;  $p < 0.0001$ ; Fig. 14a), indicating that the reformed myelin was thinner in TRPV4KO mice than in WT mice. While axon diameters showed no clear differences between WT or TRPV4KO mice (average axon diameters:  $2.188 \pm 0.038$  in WT vs.  $2.291 \pm 0.037$  in TRPV4KO;  $p = 0.053$ ), the axon diameters were significantly smaller on the ipsilateral sides in both genotypes (Fig. 14b). Scatter plots showed higher g-ratios in TRPV4KO mice in all sizes of axons at 2 months after injury, suggesting the thinner myelin in TRPV4KO mice is independent of axon size (Fig. 14c).

I further examined the recovery of sciatic nerve function during chronic stages. Walking track analysis and EM analysis were performed 6 months after sciatic nerve cut injury in both WT and TRPV4KO mice. However, I did not find any significant differences in SFI values between WT and TRPV4KO mice (Fig. 15a). Moreover, the regenerated sciatic nerves also looked similar between the two genotypes by EM (Fig. 15b), which was supported by the calculated g-ratio values and axon diameters, although axon diameters were still significantly smaller on the ipsilateral side in both genotypes (Fig. 15c, d). Taken together, these results demonstrate that the lack of TRPV4 delayed sciatic nerve remyelination and functional recovery following sciatic nerve cut-induced Wallerian degeneration.

## 5. Discussion

TRPV4 is widely expressed and functions in various glial cell types including astrocytes (49), microglia (50, 51), oligodendrocytes (52) and satellite glial cells (53). Among these cells, oligodendrocytes of the CNS have a similar function as SCs of the PNS, and satellite glial cells are of the same neural crest lineage as SCs. Here, I provide both molecular and physiological evidence showing that TRPV4 is functionally expressed in cultured mouse SCs (Fig. 1, Fig. 2), as well as in unmyelinating SCs of the sciatic nerve in mice (Fig. 4a). TRPA1 has also been identified to be expressed in SCs in a previous report (46). However, I didn't detect the functional expression of TRPA1 in my cultured SCs, though TRPA1 mRNA was detected (Fig. 3a, 3b).

Previous studies showed that  $Ca^{2+}$  signaling is an important mediator of SC differentiation during myelin development and remyelination following injury. The calcineurin/NFAT pathway is reported to be downstream of NRG1-III which is involved in activating myelination in SCs during myelin development (37, 38). TRPV4, which is co-expressed with calcineurin in many cell types, is another candidate for regulating calcineurin/NFAT signaling (69-73). However, my present results suggest that TRPV4 is not involved in SC differentiation during myelin development (Fig. 4, Fig. 5), similar to the phenomenon in oligodendrocytes of the CNS in which TRPV4 does not affect the differentiation of oligodendrocyte precursor cells (52). This is likely due to the very low expression level and activity of TRPV4 in SCs under normal conditions. Thus, loss of the TRPV4-induced increase in intracellular  $Ca^{2+}$  in TRPV4KO mice might be insufficient to block the calcineurin-NFAT pathway which further affects SC myelination, in which NRG1-III may play a major role.

I next examined the role of TRPV4 in SC differentiation following sciatic nerve cut injury. Interestingly, TRPV4 expression was increased after sciatic nerve injury (Fig. 6, Fig. 7) which is consistent with a previous report showing that expression of TRPV4 was increased in a model of cuprizone (CPZ)-induced demyelination in the corpus callosum of the CNS; however, the specific cell types were not clearly shown (74). In my results, I found that after injury in the PNS the increase in TRPV4 was mostly attributed to SCs, although TRPV4 is also expressed by invading macrophages (Fig. 7). Furthermore, I found that TRPV4 is expressed only in unmyelinating SCs, but not in myelinating SCs, which is different from the expression pattern reported for TRPV4 in

oligodendrocytes in which TRPV4 mRNA was reported to be expressed in both oligodendrocyte precursor cells and mature oligodendrocytes (52). I also verified that unmyelinating SCs are increased after nerve injury, which is well accepted, and these cells likely contribute to the increase in TRPV4 protein.

Temperature thresholds for TRPV4 activation by heat vary with the cell types in which these ion channels are expressed (48, 75). Temperature thresholds for heat-evoked TRPV4 activation are between 25°C and 33°C in HEK293 cells (76, 77), and around 27°C in *Xenopus* oocytes (76). In the present thesis, I found that TRPV4 was activated in SCs when temperature was elevated up to 37°C. While I did not determine the precise temperature threshold for channel activation, it should be lower than 33°C based on the traces (Fig. 10). Moreover, TRPV4 is known to be desensitized by temperatures above threshold, and the channels are spontaneously activated by temperatures above around 37°C (76). Taken together, this suggests that TRPV4 is constitutively active in SCs at normal body temperature.

The lack of TRPV4 caused abnormal accumulation of myelin structural proteins in the distal nerves (Fig. 11), resulting in delayed remyelination and functional recovery of sciatic nerves after injury (Fig. 12, Fig.13, Fig.14). It is interesting that TRPV4 is not involved in SC differentiation during myelin development, but is important for SC remyelination after nerve injury. I speculate that TRPV4 may have a function in SC autophagy that mediates myelin breakdown and myelin debris clearance following sciatic nerve cut-induced Wallerian degeneration, while these autophagic processes are absent during myelin development. Previous reports have suggested that TRPV4 induces autophagy in several cell types. For instance, TRPV4 induces autophagy through the AKT signaling pathway, potentially by regulating  $Ca^{2+}$  levels and osmotic pressure in hepatic stellate cells (78), and TRPV4 increases autophagy-related proteins during osteoclast differentiation by activating the  $Ca^{2+}$ -calcineurin-NFATc1 pathway (79). It is well known that the control of myelin breakdown and myelin debris clearance is a central step in nerve injury and pathology (80). Myelin debris clearance must rapidly occur over the course of 7-14 days (80-82), and robust and efficient removal of myelin debris is an important contributor to nerve regeneration and remyelination. I speculate that TRPV4 deficiency likely impairs the myelin breakdown and debris clearance function in SCs, resulting in residual myelin debris in the distal stumps after injury, and this

interferes with remyelination and functional recovery. However, sciatic nerve functional recovery and myelin morphology are similar in WT and TRPV4KO littermates 6 months after injury (Fig.15), which is probably due to some unknown compensatory process or pathway.

In addition to the basal activation of TRPV4 in SCs at physiological body temperature (37°C; Fig. 10), TRPV4 activation may also be increased by various cytokines or molecular regulators after injury. For instance, TRPV4 is capable of responding to one or more of the conditions associated with local inflammatory responses during injury, such as increased tissue temperature, reduced pH (83) and abnormal mechanical pressures due to volume changes in interstitial fluid (84). Prostaglandin E2 and serotonin can also increase the extent of TRPV4 channel activity (85), whereas serotonin and histamine have been reported to increase the expression of TRPV4 (86). Protease-activated receptor 2 signaling is another inflammatory response factor that can activate TRPV4 (87). In addition to the early stages of inflammation, some regulators also have effects on TRPV4 during the recovery stage. Activation of the PKA pathway, which is critical for promoting SC differentiation into a myelinating phenotype (88), phosphorylates specific sites on TRPV4 which increases the activity of the ion channel (89, 90). Arachidonic acid and its metabolites, which are known to be involved in the modulation of neuronal function and survival during Wallerian degeneration (91), are also well-known endogenous agonists of TRPV4. Taken together, these suggest that TRPV4 activity may be increased after injury, which causes activation of the calcineurin-NFAT pathway through the increase in intracellular calcium, and that TRPV4 plays a significant role in SC differentiation after injury.

Previous reports have suggested that TRPV4 is expressed and functions in a population of DRG neurons which may mediate nociceptive responses to hypotonic stimuli and mechanical pressure (92-94). In addition, TRPV4 was found to regulate NGF or cAMP-induced neurite outgrowth in peripheral nerves (95). In my studies, I did not examine sensory function in small diameter axons, since motor function was seriously impaired in the sciatic nerve cut injury model in these mice. Instead, I focused on the nerve recovery of the myelinated axons. TRPV4 seems not to be involved in axon degeneration and regeneration following sciatic nerve cut-induced Wallerian degeneration (Fig. 11a, Fig. 11b, Fig. 14b, Fig. 15d). This is likely due to the very low levels of TRPV4 expression in the axon terminals of DRG neurons. Cytokines or

molecular regulators secreted from the injured nerves thus fail to sensitize TRPV4 channels in the cell bodies of DRG neurons which are distant from the injury site, while the basal activity of TRPV4 is not sufficient to affect axon extension or regeneration during the recovery process.

In summary, I propose the following mechanism and schematic model of TRPV4 function in the sciatic nerve cut injury model (Fig.16). TRPV4 is mainly expressed in unmyelinating SCs. Following sciatic nerve cut injury, SCs are gradually demyelinated, resulting in an increase in TRPV4. The increased TRPV4 is activated under physiological conditions and plays a pivotal role in this process. Lack of TRPV4 leads to a large accumulation of myelin proteins at the injury site, which could inhibit remyelination. However, the reason for the greater amount of myelin structural proteins in TRPV4KO mice is still unknown. One possibility is that high levels of these structural proteins in TRPV4KO mice result from a deficiency in myelin breakdown or poor clearance of myelin debris by SCs or macrophages, which interferes with new myelin formation. Another possibility is that TRPV4 may be involved in maintaining the appropriate levels of myelin structural proteins during SC differentiation after injury, which is important for sciatic nerve remyelination. To fully understand the details of this mechanism, further investigations are required.

Thus, I conclude that TRPV4 enhances SC remyelination after sciatic nerve cut injury. My experiments used a sciatic nerve cut injury model, which mimics the neurotmesis in peripheral nerves, in which axons, connective sheaths and basal lamina tubes are interrupted. The model is the most serious nerve injury in nerve damage schemes in rodents, and it takes more than 6 months to recover, although the functional recovery is generally poor and the reformed axon and myelin are thinner than normal condition. However, it is impossible for human to be completely recovered, even though some surgical repair may help. Our studies suggest that our body temperature contributes to the natural recovery of the peripheral nerve injury by activating TRPV4, thus TRPV4 may be an attractive pharmacological target for therapeutic intervention after peripheral nerve injury.

## **6. Acknowledgments**

First, I would like to thank Prof. Nobuhiko Ohno for kindly supporting the EM analysis of myelin structure.

I would like to express my sincere gratitude to Prof. Makoto Tominaga, for the continuous support of my Ph.D. studies and related research, for his patience, motivation, and vast knowledge.

I would like to thank Dr. Yasunori Takayama. He has continuously given me good suggestions and encouragement. With his support, I overcame a lot of obstacles during my Ph.D studies.

My sincere thanks also go to all of the lab members, my housemate, and my family.

## 7. References

1. The Biology of Schwann Cells: Development, Differentiation and Immunomodulation. 2007, Cambridge University Press: Cambridge, United Kingdom.
2. Pereira JA, Lebrun-Julien F and Suter U. Molecular mechanisms regulating myelination in the peripheral nervous system. *Trends Neurosci*, 2012. **35**(2):123-134.
3. Woodhoo A and Sommer L. Development of the Schwann cell lineage: from the neural crest to the myelinated nerve. *Glia*, 2008. **56**(14):1481-1490.
4. Jessen KR and Mirsky R. The origin and development of glial cells in peripheral nerves. *Nat Rev Neurosci*, 2005. **6**(9):671-682.
5. Jessen KR, Brennan A, Morgan L, *et al.* The Schwann cell precursor and its fate: a study of cell death and differentiation during gliogenesis in rat embryonic nerves. *Neuron*, 1994. **12**(3):509-527.
6. Dong Z, Brennan A, Liu N, *et al.* Neu differentiation factor is a neuron-glia signal and regulates survival, proliferation, and maturation of rat Schwann cell precursors. *Neuron*, 1995. **15**(3):585-596.
7. Peter D and Peter KT. *Peripheral Neuropathy*. 4th ed. 2005, Elsevier Saunders: Philadelphia, PA.
8. Bozzali M and Wrabetz L. Axonal signals and oligodendrocyte differentiation. *Neurochem Res*, 2004. **29**(5):979-988.
9. Simons M and Trajkovic K. Neuron-glia communication in the control of oligodendrocyte function and myelin biogenesis. *J Cell Sci*, 2006. **119**(Pt 21):4381-4389.
10. Nave KA and Trapp BD. Axon-glia signaling and the glial support of axon function. *Annu Rev Neurosci*, 2008. **31**:535-561.
11. Sulaiman OA and Gordon T. Role of chronic Schwann cell denervation in poor functional recovery after nerve injuries and experimental strategies to combat it. *Neurosurgery*, 2009. **65**(4 Suppl):A105-114.
12. Jessen KR and Mirsky R. Negative regulation of myelination: relevance for development, injury, and demyelinating disease. *Glia*, 2008. **56**(14):1552-1565.
13. Arthur-Farraj PJ, Latouche M, Wilton DK, *et al.* c-Jun reprograms Schwann cells of injured

- nerves to generate a repair cell essential for regeneration. *Neuron*, 2012. **75**(4):633-647.
14. Hirata K and Kawabuchi M. Myelin phagocytosis by macrophages and nonmacrophages during Wallerian degeneration. *Microsc Res Tech*, 2002. **57**(6):541-547.
  15. Rotshenker S. Wallerian degeneration: the innate-immune response to traumatic nerve injury. *J Neuroinflammation*, 2011. **8**:109.
  16. Vidal PM, Lemmens E, Dooley D, *et al.* The role of "anti-inflammatory" cytokines in axon regeneration. *Cytokine Growth Factor Rev*, 2013. **24**(1):1-12.
  17. Gomez-Sanchez JA, Carty L, Iruarrizaga-Lejarreta M, *et al.* Schwann cell autophagy, myelinophagy, initiates myelin clearance from injured nerves. *J Cell Biol*, 2015. **210**(1):153-168.
  18. Barrette B, Hebert MA, Filali M, *et al.* Requirement of myeloid cells for axon regeneration. *J Neurosci*, 2008. **28**(38):9363-9376.
  19. Topilko P, Schneider-Maunoury S, Levi G, *et al.* Krox-20 controls myelination in the peripheral nervous system. *Nature*, 1994. **371**(6500):796-799.
  20. Le N, Nagarajan R, Wang JY, *et al.* Nab proteins are essential for peripheral nervous system myelination. *Nat Neurosci*, 2005. **8**(7):932-940.
  21. Salzer JL. Schwann cell myelination. *Cold Spring Harb Perspect Biol*, 2015. **7**(8):a020529.
  22. Parkinson DB, Bhaskaran A, Arthur-Farraj P, *et al.* c-Jun is a negative regulator of myelination. *J Cell Biol*, 2008. **181**(4):625-637.
  23. Jessen KR, Mirsky R and Lloyd AC. Schwann Cells: Development and Role in Nerve Repair. *Cold Spring Harb Perspect Biol*, 2015. **7**(7):a020487.
  24. Birchmeier C and Nave KA. Neuregulin-1, a key axonal signal that drives Schwann cell growth and differentiation. *Glia*, 2008. **56**(14):1491-1497.
  25. Taveggia C, Zanazzi G, Petrylak A, *et al.* Neuregulin-1 type III determines the ensheathment fate of axons. *Neuron*, 2005. **47**(5):681-694.
  26. Boerboom A, Dion V, Chariot A, *et al.* Molecular Mechanisms Involved in Schwann Cell Plasticity. *Front Mol Neurosci*, 2017. **10**:38.
  27. Woodhoo A, Alonso MB, Droggiti A, *et al.* Notch controls embryonic Schwann cell differentiation, postnatal myelination and adult plasticity. *Nat Neurosci*, 2009. **12**(7):839-847.

28. Wang J, Ren KY, Wang YH, *et al.* Effect of active Notch signaling system on the early repair of rat sciatic nerve injury. *Artif Cells Nanomed Biotechnol*, 2015. **43**(6):383-389.
29. Napoli I, Noon LA, Ribeiro S, *et al.* A central role for the ERK-signaling pathway in controlling Schwann cell plasticity and peripheral nerve regeneration in vivo. *Neuron*, 2012. **73**(4):729-742.
30. Nosedá R, Belin S, Piguet F, *et al.* DDIT4/REDD1/RTP801 is a novel negative regulator of Schwann cell myelination. *J Neurosci*, 2013. **33**(38):15295-15305.
31. Norrmen C and Suter U. Akt/mTOR signalling in myelination. *Biochem Soc Trans*, 2013. **41**(4):944-950.
32. Morton PD, Johnstone JT, Ramos AY, *et al.* Nuclear factor-kappaB activation in Schwann cells regulates regeneration and remyelination. *Glia*, 2012. **60**(4):639-650.
33. Morton PD, Dellarole A, Theus MH, *et al.* Activation of NF-kappaB in Schwann cells is dispensable for myelination in vivo. *J Neurosci*, 2013. **33**(24):9932-9936.
34. Shin YK, Jang SY, Park JY, *et al.* The Neuregulin-Rac-MKK7 pathway regulates antagonistic c-jun/Krox20 expression in Schwann cell dedifferentiation. *Glia*, 2013. **61**(6):892-904.
35. Yang DP, Kim J, Syed N, *et al.* p38 MAPK activation promotes denervated Schwann cell phenotype and functions as a negative regulator of Schwann cell differentiation and myelination. *J Neurosci*, 2012. **32**(21):7158-7168.
36. Roberts SL, Dun XP, Dee G, *et al.* The role of p38alpha in Schwann cells in regulating peripheral nerve myelination and repair. *J Neurochem*, 2017. **141**(1):37-47.
37. Taveggia C, Feltri ML and Wrabetz L. Signals to promote myelin formation and repair. *Nat Rev Neurol*, 2010. **6**(5):276-287.
38. Kao SC, Wu H, Xie J, *et al.* Calcineurin/NFAT signaling is required for neuregulin-regulated Schwann cell differentiation. *Science*, 2009. **323**(5914):651-654.
39. Ino D, Sagara H, Suzuki J, *et al.* Neuronal Regulation of Schwann Cell Mitochondrial Ca(2+) Signaling during Myelination. *Cell Rep*, 2015. **12**(12):1951-1959.
40. Stevens B and Fields RD. Response of Schwann cells to action potentials in development. *Science*, 2000. **287**(5461):2267-2271.
41. Carrer A, Leparulo A, Crispino G, *et al.* Cx32 hemichannel opening by cytosolic Ca<sup>2+</sup> is inhibited by the R220X mutation that causes Charcot-Marie-Tooth disease. *Hum Mol Genet*,

2018. **27**(1):80-94.
42. Coover RA, Healy TE, Guo L, *et al.* Tonic ATP-mediated growth suppression in peripheral nerve glia requires arrestin-PP2 and is evaded in NF1. *Acta Neuropathol Commun*, 2018. **6**(1):127.
  43. Baraban M, Koudelka S and Lyons DA. Ca (2+) activity signatures of myelin sheath formation and growth in vivo. *Nat Neurosci*, 2018. **21**(1):19-23.
  44. Flockerzi V and Nilius B. *Transient Receptor Potential (TRP) Channels*. 2007, Springer-Verlag Berlin Heidelberg: Berlin, Heidelberg.
  45. Hamilton NB, Kolodziejczyk K, Kougioumtzidou E, *et al.* Proton-gated Ca(2+)-permeable TRP channels damage myelin in conditions mimicking ischaemia. *Nature*, 2016. **529**(7587):523-527.
  46. De Logu F, Nassini R, Materazzi S, *et al.* Schwann cell TRPA1 mediates neuroinflammation that sustains macrophage-dependent neuropathic pain in mice. *Nat Commun*, 2017. **8**(1):1887.
  47. Watanabe H, Vriens J, Prenen J, *et al.* Anandamide and arachidonic acid use epoxyeicosatrienoic acids to activate TRPV4 channels. *Nature*, 2003. **424**(6947):434-438.
  48. White JP, Cibelli M, Urban L, *et al.* TRPV4: Molecular Conductor of a Diverse Orchestra. *Physiol Rev*, 2016. **96**(3):911-973.
  49. Shibasaki K, Ikenaka K, Tamalu F, *et al.* A novel subtype of astrocytes expressing TRPV4 (transient receptor potential vanilloid 4) regulates neuronal excitability via release of gliotransmitters. *J Biol Chem*, 2014. **289**(21):14470-14480.
  50. Shirakawa H, Nakagawa T and Kaneko S. Pathophysiological roles of transient receptor potential channels in glial cells. *Yakugaku Zasshi*, 2010. **130**(3):281-287.
  51. Konno M, Shirakawa H, Iida S, *et al.* Stimulation of transient receptor potential vanilloid 4 channel suppresses abnormal activation of microglia induced by lipopolysaccharide. *Glia*, 2012. **60**(5):761-770.
  52. Ohashi K, Deyashiki A, Miyake T, *et al.* TRPV4 is functionally expressed in oligodendrocyte precursor cells and increases their proliferation. *Pflugers Arch*, 2018. **470**(5):705-716.
  53. Rajasekhar P, Poole DP, Liedtke W, *et al.* P2Y1 Receptor Activation of the TRPV4 Ion Channel Enhances Purinergic Signaling in Satellite Glial Cells. *J Biol Chem*, 2015.

**290(48):29051-29062.**

54. Mizuno A, Matsumoto N, Imai M, *et al.* Impaired osmotic sensation in mice lacking TRPV4. *Am J Physiol Cell Physiol*, 2003. **285(1):C96-101.**
55. Honkanen H, Lahti O, Nissinen M, *et al.* Isolation, purification and expansion of myelination-competent, neonatal mouse Schwann cells. *Eur J Neurosci*, 2007. **26(4):953-964.**
56. Morrissey TK, Kleitman N and Bunge RP. Isolation and functional characterization of Schwann cells derived from adult peripheral nerve. *J Neurosci*, 1991. **11(8):2433-2442.**
57. Monje PV, Soto J, Bacallao K, *et al.* Schwann cell dedifferentiation is independent of mitogenic signaling and uncoupled to proliferation: role of cAMP and JNK in the maintenance of the differentiated state. *J Biol Chem*, 2010. **285(40):31024-31036.**
58. Zhou R and Mei L. *Neural Development: Methods and Protocols*. 2013, Humana Press: New York, United States.
59. Takayama Y, Shibasaki K, Suzuki Y, *et al.* Modulation of water efflux through functional interaction between TRPV4 and TMEM16A/anoctamin 1. *Faseb j*, 2014. **28(5):2238-2248.**
60. Krinke GJ, Vidotto N and Weber E. Teased-fiber technique for peripheral myelinated nerves: methodology and interpretation. *Toxicol Pathol*, 2000. **28(1):113-121.**
61. Sung MA, Jung HJ, Lee JW, *et al.* Human umbilical cord blood-derived mesenchymal stem cells promote regeneration of crush-injured rat sciatic nerves. *Neural Regen Res*, 2012. **7(26):2018-2027.**
62. Inserra MM, Bloch DA and Terris DJ. Functional indices for sciatic, peroneal, and posterior tibial nerve lesions in the mouse. *Microsurgery*, 1998. **18(2):119-124.**
63. Chamberlain LJ, Yannas IV, Hsu HP, *et al.* Near-terminus axonal structure and function following rat sciatic nerve regeneration through a collagen-GAG matrix in a ten-millimeter gap. *J Neurosci Res*, 2000. **60(5):666-677.**
64. Ohno N, Kidd GJ, Mahad D, *et al.* Myelination and axonal electrical activity modulate the distribution and motility of mitochondria at CNS nodes of Ranvier. *J Neurosci*, 2011. **31(20):7249-7258.**
65. Thai TQ, Nguyen HB, Saitoh S, *et al.* Rapid specimen preparation to improve the throughput of electron microscopic volume imaging for three-dimensional analyses of subcellular

- ultrastructures with serial block-face scanning electron microscopy. *Med Mol Morphol*, 2016. **49**(3):154-162.
66. Yang Z and Wang KK. Glial fibrillary acidic protein: from intermediate filament assembly and gliosis to neurobiomarker. *Trends Neurosci*, 2015. **38**(6):364-374.
67. Shibasaki K, Suzuki M, Mizuno A, *et al.* Effects of body temperature on neural activity in the hippocampus: regulation of resting membrane potentials by transient receptor potential vanilloid 4. *J Neurosci*, 2007. **27**(7):1566-1575.
68. Shibasaki K, Sugio S, Takao K, *et al.* TRPV4 activation at the physiological temperature is a critical determinant of neuronal excitability and behavior. *Pflugers Arch*, 2015. **467**(12):2495-2507.
69. Masuyama R, Vriens J, Voets T, *et al.* TRPV4-mediated calcium influx regulates terminal differentiation of osteoclasts. *Cell Metab*, 2008. **8**(3):257-265.
70. Wang Z, Wang Y, Tian X, *et al.* Transient receptor potential channel 1/4 reduces subarachnoid hemorrhage-induced early brain injury in rats via calcineurin-mediated NMDAR and NFAT dephosphorylation. *Sci Rep*, 2016. **6**:33577.
71. Li M, Fang XZ, Zheng YF, *et al.* Transient receptor potential vanilloid 4 is a critical mediator in LPS mediated inflammation by mediating calcineurin/NFATc3 signaling. *Biochem Biophys Res Commun*, 2019. **513**(4):1005-1012.
72. Zhao L, Sullivan MN, Chase M, *et al.* Calcineurin/nuclear factor of activated T cells-coupled vanilloid transient receptor potential channel 4  $Ca^{2+}$  sparklets stimulate airway smooth muscle cell proliferation. *Am J Respir Cell Mol Biol*, 2014. **50**(6):1064-1075.
73. Masuyama R, Mizuno A, Komori H, *et al.* Calcium/calmodulin-signaling supports TRPV4 activation in osteoclasts and regulates bone mass. *J Bone Miner Res*, 2012. **27**(8):1708-1721.
74. Liu M, Liu X, Wang L, *et al.* TRPV4 Inhibition Improved Myelination and Reduced Glia Reactivity and Inflammation in a Cuprizone-Induced Mouse Model of Demyelination. *Front Cell Neurosci*, 2018. **12**:392.
75. Wolfgang BL and Stefan H. TRP ion channel function in sensory transduction and cellular signaling cascades. 2006, CRC Press: Florida, United States.
76. Guler AD, Lee H, Iida T, *et al.* Heat-evoked activation of the ion channel, TRPV4. *J Neurosci*,

2002. **22**(15):6408-6414.
77. Watanabe H, Vriens J, Suh SH, *et al.* Heat-evoked activation of TRPV4 channels in a HEK293 cell expression system and in native mouse aorta endothelial cells. *J Biol Chem*, 2002. **277**(49):47044-47051.
78. Cao B, Dai X and Wang W. Knockdown of TRPV4 suppresses osteoclast differentiation and osteoporosis by inhibiting autophagy through Ca(2+) -calcineurin-NFATc1 pathway. *J Cell Physiol*, 2019. **234**(5):6831-6841.
79. Zhan L, Yang Y, Ma TT, *et al.* Transient receptor potential vanilloid 4 inhibits rat HSC-T6 apoptosis through induction of autophagy. *Mol Cell Biochem*, 2015. **402**(1-2):9-22.
80. Vargas ME and Barres BA. Why is Wallerian degeneration in the CNS so slow? *Annu Rev Neurosci*, 2007. **30**:153-179.
81. Griffin JW, George R, Lobato C, *et al.* Macrophage responses and myelin clearance during Wallerian degeneration: relevance to immune-mediated demyelination. *J Neuroimmunol*, 1992. **40**(2-3):153-165.
82. George R and Griffin JW. Delayed macrophage responses and myelin clearance during Wallerian degeneration in the central nervous system: the dorsal radiclotomy model. *Exp Neurol*, 1994. **129**(2):225-236.
83. Shikano M, Ueda T, Kamiya T, *et al.* Acid inhibits TRPV4-mediated Ca(2+)(+) influx in mouse esophageal epithelial cells. *Neurogastroenterol Motil*, 2011. **23**(11):1020-1028, e1497.
84. White JP, Cibelli M, Rei Fidalgo A, *et al.* Role of transient receptor potential and acid-sensing ion channels in peripheral inflammatory pain. *Anesthesiology*, 2010. **112**(3):729-741.
85. Chen X, Alessandri-Haber N and Levine JD. Marked attenuation of inflammatory mediator-induced C-fiber sensitization for mechanical and hypotonic stimuli in TRPV4-/- mice. *Mol Pain*, 2007. **3**:31.
86. Cenac N, Altier C, Motta JP, *et al.* Potentiation of TRPV4 signalling by histamine and serotonin: an important mechanism for visceral hypersensitivity. *Gut*, 2010. **59**(4):481-488.
87. Grant AD, Cottrell GS, Amadesi S, *et al.* Protease-activated receptor 2 sensitizes the transient receptor potential vanilloid 4 ion channel to cause mechanical hyperalgesia in mice. *J Physiol*, 2007. **578**(Pt 3):715-733.
88. Yoon C, Korade Z and Carter BD. Protein kinase A-induced phosphorylation of the p65

- subunit of nuclear factor-kappaB promotes Schwann cell differentiation into a myelinating phenotype. *J Neurosci*, 2008. **28**(14):3738-3746.
89. Fan HC, Zhang X and Mcnaughton PA. Activation of the TRPV4 ion channel is enhanced by phosphorylation. *J Biol Chem*, 2009. **284**(41):27884-27891.
90. Peng H, Lewandrowski U, Muller B, *et al.* Identification of a Protein Kinase C-dependent phosphorylation site involved in sensitization of TRPV4 channel. *Biochem Biophys Res Commun*, 2010. **391**(4):1721-1725.
91. Camara-Lemarroy CR, Gonzalez-Moreno EI, Guzman-De La Garza FJ, *et al.* Arachidonic acid derivatives and their role in peripheral nerve degeneration and regeneration. *ScientificWorldJournal*, 2012. **2012**:168953.
92. Alessandri-Haber N, Yeh JJ, Boyd AE, *et al.* Hypotonicity induces TRPV4-mediated nociception in rat. *Neuron*, 2003. **39**(3):497-511.
93. Suzuki M, Mizuno A, Kodaira K, *et al.* Impaired pressure sensation in mice lacking TRPV4. *J Biol Chem*, 2003. **278**(25):22664-22668.
94. Suzuki M, Watanabe Y, Oyama Y, *et al.* Localization of mechanosensitive channel TRPV4 in mouse skin. *Neurosci Lett*, 2003. **353**(3):189-192.
95. Jang Y, Jung J, Kim H, *et al.* Axonal neuropathy-associated TRPV4 regulates neurotrophic factor-derived axonal growth. *J Biol Chem*, 2012. **287**(8):6014-6024.

## 8. Figure Legends

### Figure 1. TRPV4 expression in cultured mouse Schwann cells

- (a) Characterization of purified Schwann cells (SCs) from sciatic nerves of postnatal day 1 (P1) wild-type (WT) mice using a fluorescence microscope. After complement-mediated cytolysis, cultures were double-labeled with DAPI (blue) and S100 $\beta$  (red), a marker of SCs. The left panel shows the bright-field image and the right panel shows the merged image of S100 and DAPI double-staining. Scale bars: 100  $\mu$ m.
- (b) RT-PCR for TRPV4 mRNA expression in purified primary SCs from P1 and adult mice. The negative control (-) was run without reverse transcriptase treatment.  $\beta$ -actin mRNA (*Actb*) was used as a loading control. The expected sizes of *Trpv4* and *Actb* are 404 bp and 573 bp, respectively.
- (c) Western blotting of TRPV4 in purified primary SCs from P1 WT and TRPV4KO mice. Vinculin bands represent the loading control. The predicted molecular weights of TRPV4 and vinculin are 100 kDa and 117 kDa, respectively.

### Figure 2. Functional expression of TRPV4 in cultured mouse Schwann cells

- (a, b) Mean Fura-2 ratios corresponding to the intracellular Ca<sup>2+</sup> concentrations in primary SCs isolated from adult WT (a) or TRPV4KO mice (b). (a) SCs were stimulated with GSK1016790A (GSK, 1.0  $\mu$ M), a TRPV4-selective agonist, in the presence or absence of 2.0 mM extracellular Ca<sup>2+</sup> (n = 50 cells). Ionomycin (iono, 5.0  $\mu$ M) was applied to confirm cell viability. (b) SCs were stimulated with 1.0  $\mu$ M GSK in the presence of 2.0 mM extracellular Ca<sup>2+</sup> in primary TRPV4KO SCs (n = 121 cells). Data are presented as the mean  $\pm$  SEM.
- (c) Representative traces of GSK-induced currents in primary SCs from adult WT mice using a whole-cell patch-clamp method (left). Holding potential was -60 mV, and ramp-pulses from -100 to +100 mV (inset) were applied for 300 ms every 5 sec. Current-voltage (I-V) curves at the time points indicated by the colored triangles are shown at right.

### Figure 3. Expression of TRP channels in cultured mouse Schwann cells

- (a) RT-PCR for mRNA expression of TRPV1, TRPV2, TRPV3, TRPV4, TRPV5, TRPA1 and TRPM3 in

purified primary SCs from P1-3 mice. (+) and (-) represent with and without a reverse transcriptase treatment during the preparation of cDNA samples, respectively. "c" represents a positive control with a plasmid DNA as a DNA template in the reverse transcription.  $\beta$ -actin mRNA (*Actb*) was used as a loading control. The expected sizes of TRPV1, TRPV2, TRPV3, TRPV4, TRPV5, TRPA1, TRPM3 and *Actb* are 548bp, 552bp, 523bp, 404bp, 464bp, 590bp, 577bp, 556bp and 573 bp, respectively.

(b-e) Mean Fura-2 ratios corresponding to the intracellular  $\text{Ca}^{2+}$  concentrations in primary SCs isolated from P1-3 mice. Capsaicin, allyl isothiocyanate (AITC), camphor, pregnenolone sulfate (PS) and lysophosphatidylcholine (LPC) are agonists of TRPV1, TRPA1, TRPV3, TRPM3 and TRPV2, respectively. SCs were stimulated with capsaicin, AITC (b, n=30 cells), camphor, PS (c, n=27 cells), LPC (d, n=114 cells) and GSK (e, n=77 cells) with the indicated concentrations in the presence of 2.0 mM extracellular  $\text{Ca}^{2+}$ . Data are presented as the mean  $\pm$  SEM.

#### **Figure 4. Expression of myelin structural proteins in sciatic nerves from WT and TRPV4KO mice**

- (a) Western blotting of TRPV4 in sciatic nerves from 15-week-old WT and TRPV4KO mice. GAPDH bands represent the loading control. The predicted molecular weights of TRPV4 and GAPDH are 100 kDa and 37 kDa, respectively.
- (b) Immunostaining images of P0 (green), MBP (green) and MAG (red) expression in longitudinal sections of sciatic nerves from 15-week-old WT (top) and TRPV4KO (bottom) mice. Scale bars: 40  $\mu\text{m}$ .
- (c) Western blotting of neurofilament 160 (NF), MAG and P0 in sciatic nerves from 15-week-old WT and TRPV4KO littermates. The predicted molecular weights of NF, MAG and P0 are 160 kDa, 100 kDa and 25 kDa, respectively.

#### **Figure 5. Comparison of the expression of MAG and P0 proteins during the development of mouse sciatic nerves**

Representative western blot images of MAG and P0 in the sciatic nerves from postnatal day 7 (P7, a, left), postnatal day 15 (P15, b, left) postnatal day 21 (P21, c, left) and 8-week-old mice (d, left) from WT and TRPV4KO littermates. Expression levels normalized to GAPDH are shown at

right. Data are presented as the mean  $\pm$  SEM. A two-tailed *t*-test was used for comparison. ns. = not significant.

**Figure 6. Changes in the expression of NF, MAG, P0 and TRPV4 proteins in a mouse model of sciatic nerve cut injury**

- (a) Typical photographs of sciatic nerve in cut injury model. The sciatic nerve was exposed and cut (arrowhead) at the notch site (arrow) in 15-week-old mice. Distal sciatic nerves were collected for the following experiments.
- (b) Time course of the change in expression of NF, MAG and P0 proteins in WT sciatic nerves between 5 days (D5) and 5 weeks (D35) after injury.
- (c) Time-course of the change in expression of TRPV4 and MAG proteins in WT sciatic nerves between 2 days (D2) and 3 weeks (D21) after injury.

**Figure 7. Changes in the expression of NF, MAG, c-Jun, Krox20 and TRPV4 proteins in cultured mouse sciatic nerve segments**

- (a) A schematic illustration showing the expression of TRPV4 in unmyelinating SCs and macrophages after injury.
- (b) Experimental protocol for the incubation and measurement of protein expression levels in sciatic nerve segments from 15-week-old WT and TRPV4KO mice.
- (c) Comparison of the expression of NF, MAG, c-Jun, Krox20 and TRPV4 proteins in the cultured sciatic nerve segments shown in (b) from WT and TRPV4KO mice. ‘Control’ represents uncultured sciatic nerve segments; ‘D7’ represents sciatic nerve segments cultured for 7 days.

**Figure 8. Expression of TRPV4 in unmyelinating Schwann cells from teased sciatic nerves**

- (a) Immunostaining images of TRPV4 (green), GFAP (red) and DAPI (blue) in nerve fibers teased apart from the sciatic nerve of 15-week-old WT mice. The left lower panel shows the bright-field image. Scale bars: 10  $\mu$ m.
- (b) Immunostaining images of TRPV4 (green), MBP (red) and DAPI (blue) in nerve fibers teased apart from the sciatic nerve of 15-week-old WT mice. The left lower panel shows the

bright-field image. Scale bars: 10  $\mu\text{m}$ .

**Figure 9. Unmyelinating Schwann cells are increased in distal sciatic nerves 7 days after injury**

Immunostaining images of GFAP (green) and DAPI (blue) in longitudinal sciatic nerve sections from 15-week-old WT mice. The two lower images represent the negative control without primary antibody. Scale bars: 50  $\mu\text{m}$ .

**Figure 10. Body temperature-induced changes in intracellular  $\text{Ca}^{2+}$  concentrations in Schwann cells from WT and TRPV4KO mice**

Mean Fura-2 ratios corresponding to intracellular  $\text{Ca}^{2+}$  concentrations in response to temperature elevation up to 37°C in primary SCs isolated from adult WT (a; n = 33 cells) or TRPV4KO (b; n = 51 cells) mice. The lower traces (red) represent the real-time temperature during calcium imaging. 1.0  $\mu\text{M}$  GSK was applied as a positive control for the TRPV4 response. Data are presented as the mean  $\pm$  SEM.

**Figure 11. Changes in the expression of P0, NF, MAG and MBP proteins in WT and TRPV4KO mice after injury**

- (a) Time course of the changes in expression of P0 and NF160 proteins in sciatic nerves between 5 days (D5) and 2 months after injury in 15-week-old WT and TRPV4KO mice. 'Uninjured' indicates the expression in sciatic nerves without injury. 'Sham' indicates the expression in sciatic nerves that were exposed, but not cut.
- (b) Time course of the changes in expression of P0, MAG, MBP and NF160 proteins in the contralateral and ipsilateral sciatic nerves from 15-week-old WT and TRPV4KO mice at 7 days after injury. Representative western blots are presented.
- (c) Normalized expression levels (to GAPDH) of the proteins shown in (b). Data are presented as the mean (from more than 6 samples)  $\pm$  SEM. A two-tailed *t*-test was used for comparison.  
\*\*  $P < 0.01$ , ns. = not significant.

**Figure 12. TRPV4-dependent sciatic nerve function 2 months after injury**

- (a) Representative shapes of the ipsilateral hind paws from WT and TRPV4KO mice at 2 months

after injury. The WT mice had paws with spread toes, whereas most of the TRPV4KO mice showed severe contracture (4/6).

- (b) Design of the custom box used in the walking track analysis. Mice were placed at the entrance of a corridor which contained a darkened box at the end. The floor of the corridor was covered with paper tape. Hind paws of the mice were painted with black ink, and mice walked straight through the corridor into the darkened box, leaving their footprints on the paper.
- (c) Representative footprint stamps from the walking track analysis of WT and TRPV4KO mice. The red lines display ETS, NTS, EPL and NPL measurements from WT and TRPV4KO mice. PL: print length, TS: toe spread, E: experimental side (representing the ipsilateral paw), and N: normal side (representing the contralateral paw).
- (d) Quantification of sciatic nerve function using the sciatic functional index (SFI) in WT and TRPV4KO mice (n = 6 mice each). SFI values were calculated using the formula below:

$$\text{Sciatic Functional Index (SFI)} = 118.9 \left( \frac{\text{ETS} - \text{NTS}}{\text{NTS}} \right) - 51.2 \left( \frac{\text{EPL} - \text{NPL}}{\text{NPL}} \right) - 7.5$$

Data are presented as the mean  $\pm$  SEM. \*\* p<0.01.

### **Figure 13. Electron micrographs of distal sciatic nerves at 2 months after injury**

Representative transmission electron microscopy (TEM) images of transverse sections from WT contralateral (top left), WT ipsilateral (top right), TRPV4KO contralateral (lower left), and TRPV4KO ipsilateral (lower right) distal sciatic nerves at 2 months after injury. White arrowheads indicate the apparently thinner myelin sheaths in the ipsilateral sciatic nerves from TRPV4KO mice compared with WT mice. Scale bars: 5  $\mu$ m.

### **Figure 14. Comparison of parameters obtained by electron micrographs of distal sciatic nerves at 2 months after injury**

- (a) Average g-ratios of the contralateral (n = 70 axons for WT, and n = 140 for TRPV4KO mice) and ipsilateral (n = 707 axons for WT, and n = 728 for TRPV4KO mice) distal sciatic nerves in WT mice (n=3) and TRPV4KO mice (n=3) at 2 months after injury. Data are presented as the mean  $\pm$  SEM. A two-tailed t-test was used for comparison. \*\* P<0.01, ns. = not significant.

- (b) Average axon diameters of the contralateral and ipsilateral distal sciatic nerves shown in (a). Data are presented as the mean  $\pm$  SEM. A two-tailed *t*-test was used for comparison. ns. = not significant.
- (c) Scatter plots showing the g-ratios of individually measured axons. G-ratios (y-axis) are plotted against their axonal diameters (x-axis).

**Figure 15. Analysis of TRPV4-dependent sciatic nerve function and electron micrographs of distal sciatic nerves at 6 months after injury**

- (a) Quantification of sciatic nerve function by SFI in WT and TRPV4KO mice (n = 6 mice each). Data are presented as the mean  $\pm$  SEM. ns. = not significant
- (b) Representative TEM images of transverse sections of distal sciatic nerves from WT ipsilateral (left) and TRPV4KO ipsilateral (right; n = 4 mice each) at 6 months after injury. Scale bars: 5  $\mu$ m.
- (c) Comparison of the average g-ratios of ipsilateral distal sciatic nerves in WT (n = 231 axons) and TRPV4KO (n = 283 axons) mice. A two-tailed *t*-test was used for comparison. ns. = not significant.
- (d) Comparison of the axon diameters of contralateral and ipsilateral distal sciatic nerves shown in (c). A two-tailed *t*-test was used for comparison. ns. = not significant.

**Figure 16. A Proposed TRPV4 function in Schwann cells in the sciatic nerve cut injury model**

TRPV4 is expressed in unmyelinating SCs. SCs from the distal nerve are gradually demyelinated after sciatic nerve cut injury, which causes an increase in unmyelinating SCs, leading to an increase in TRPV4 protein. The increased TRPV4 is activated under physiological conditions and plays a role in SC remyelination. Lack of TRPV4 leads to a large accumulation of myelin structural proteins at the injury site which may inhibit remyelination, contributing to the more severe phenotype in TRPV4KO mice.

## 9. Tables and Figures

**Table 1**

Primer list for reverse transcription-PCR (RT-PCR).

All primers span an exon-exon junction.

<b>Gene</b>	<b>Forward primer</b>	<b>Reverse primer</b>
<i>TRPV1</i>	AACTCCACCCCACACTGAAG	TCGCCTCTGCAGGAAATACT
<i>TRPV2</i>	ACCGCATGGTGGTTTTAGAG	CTACAGCAAAGCCGAAAAGG
<i>TRPV3</i>	CATCACCTGACCCTTGTCT	GCTGAAGCTGCCATAGGAAC
<i>TRPV4</i>	ACAACACCCGAGAGAACACC	CCCAAACCTTACGCCACTTGT
<i>TRPV5</i>	GAGTTGGTGCCTCTCGCTAC	GGCAAAGGTGGCATAGGTAA
<i>TRPV6</i>	TCATTGAGCATGGAGCTGAC	GGTCACATAGGCCTCCTGAA
<i>TRPA1</i>	AACTCCTCAACCACCCTGTG	CTGAGGCCAAAAGCCAGTAG
<i>TRPM3</i>	GCCATTCTCTTTCCCAATGA	ACGAATTGAAGCGATCATCC
<i><math>\beta</math>-actin</i>	TGTTACCAACTGGGACGACA	AAGGAAGGCTGGAAAAGAGC

**Figure 1**

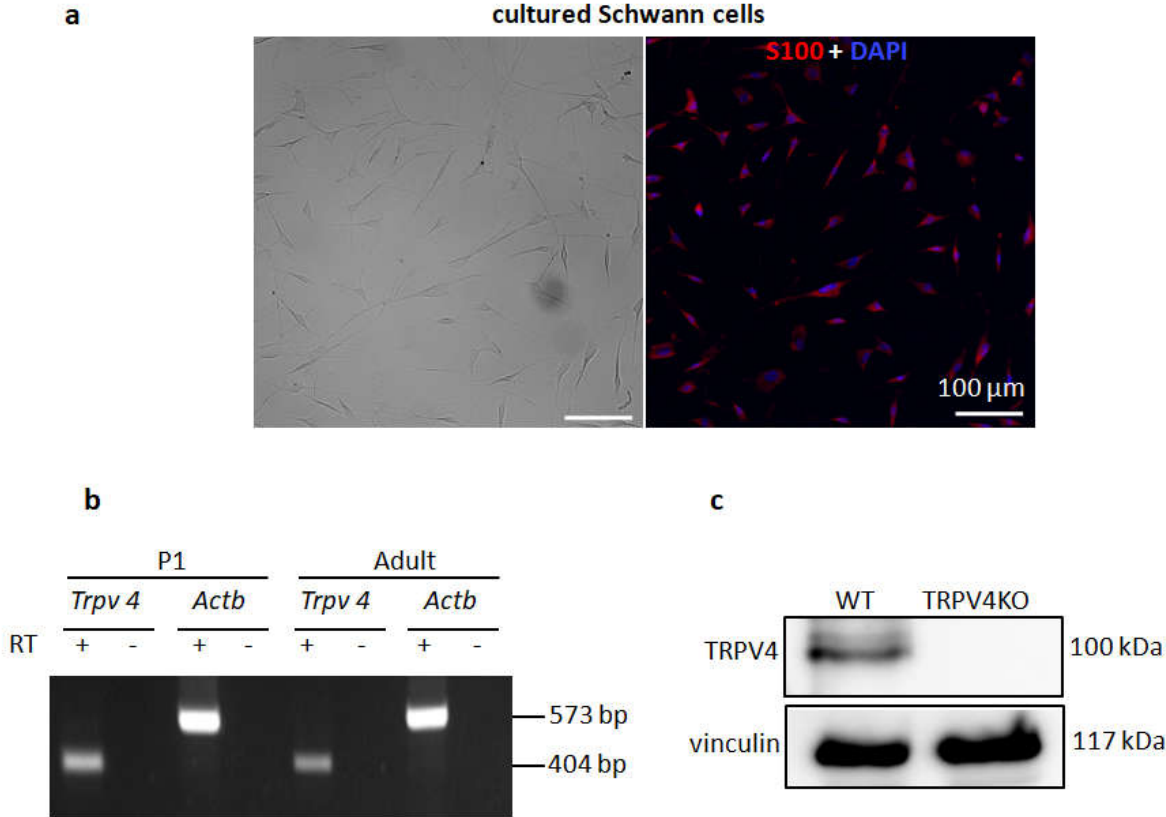
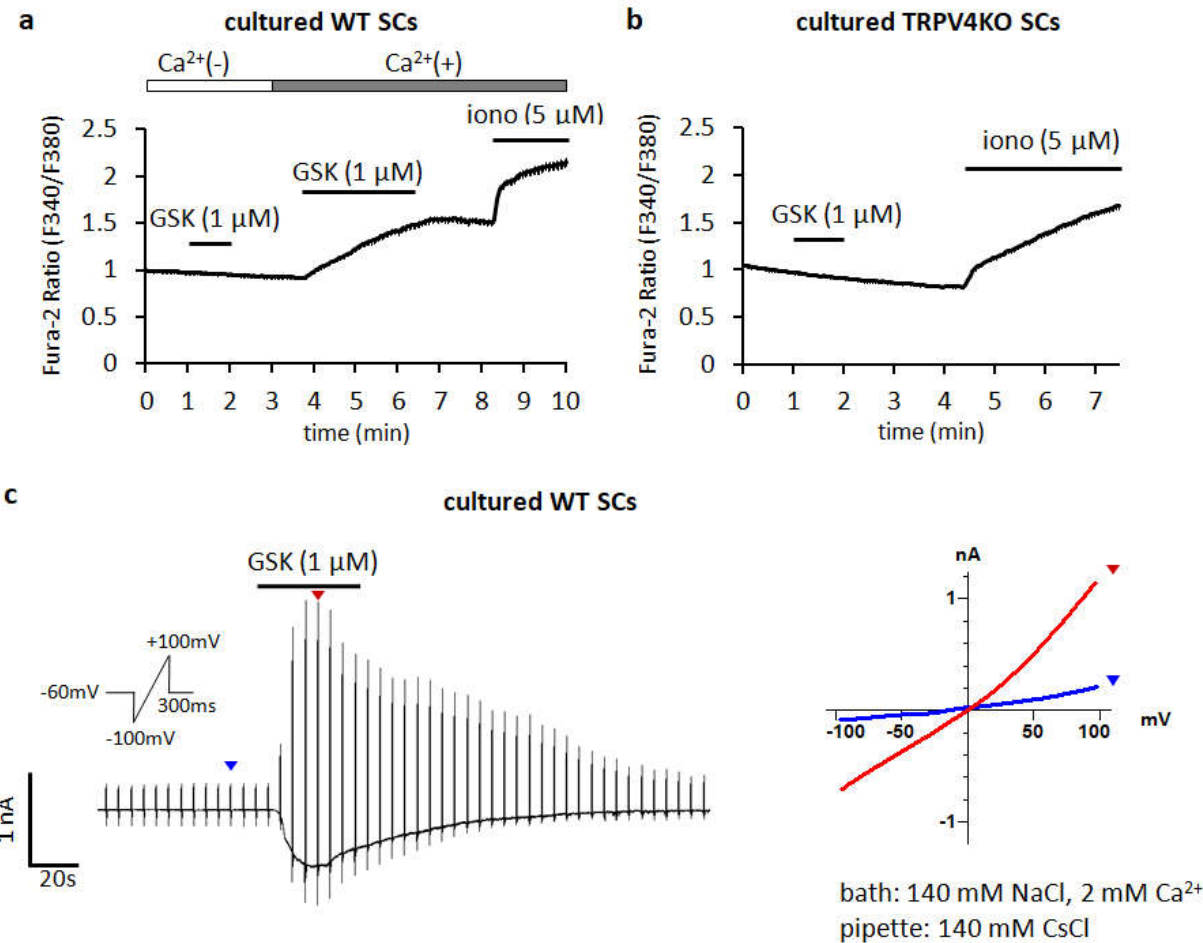
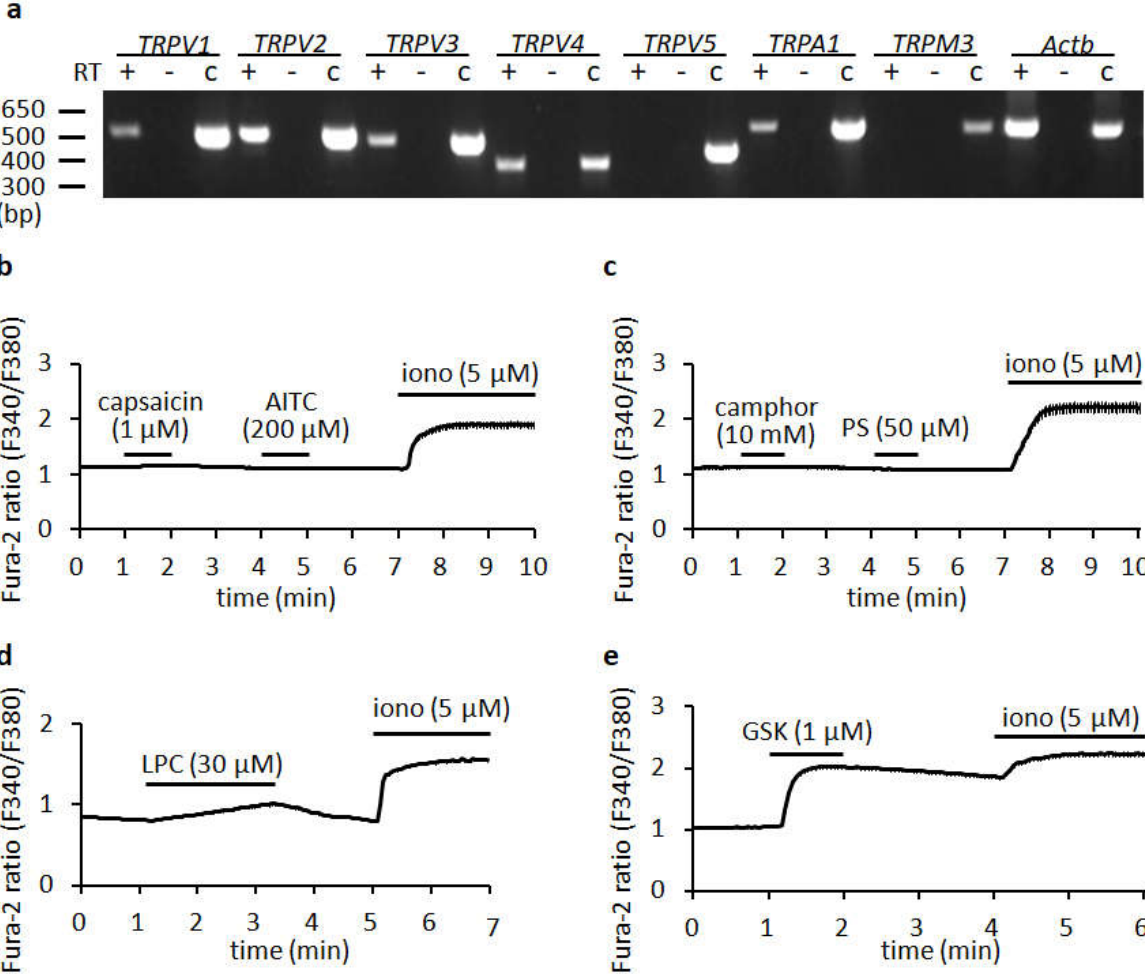


Figure 2



**Figure 3**



**Figure 4**

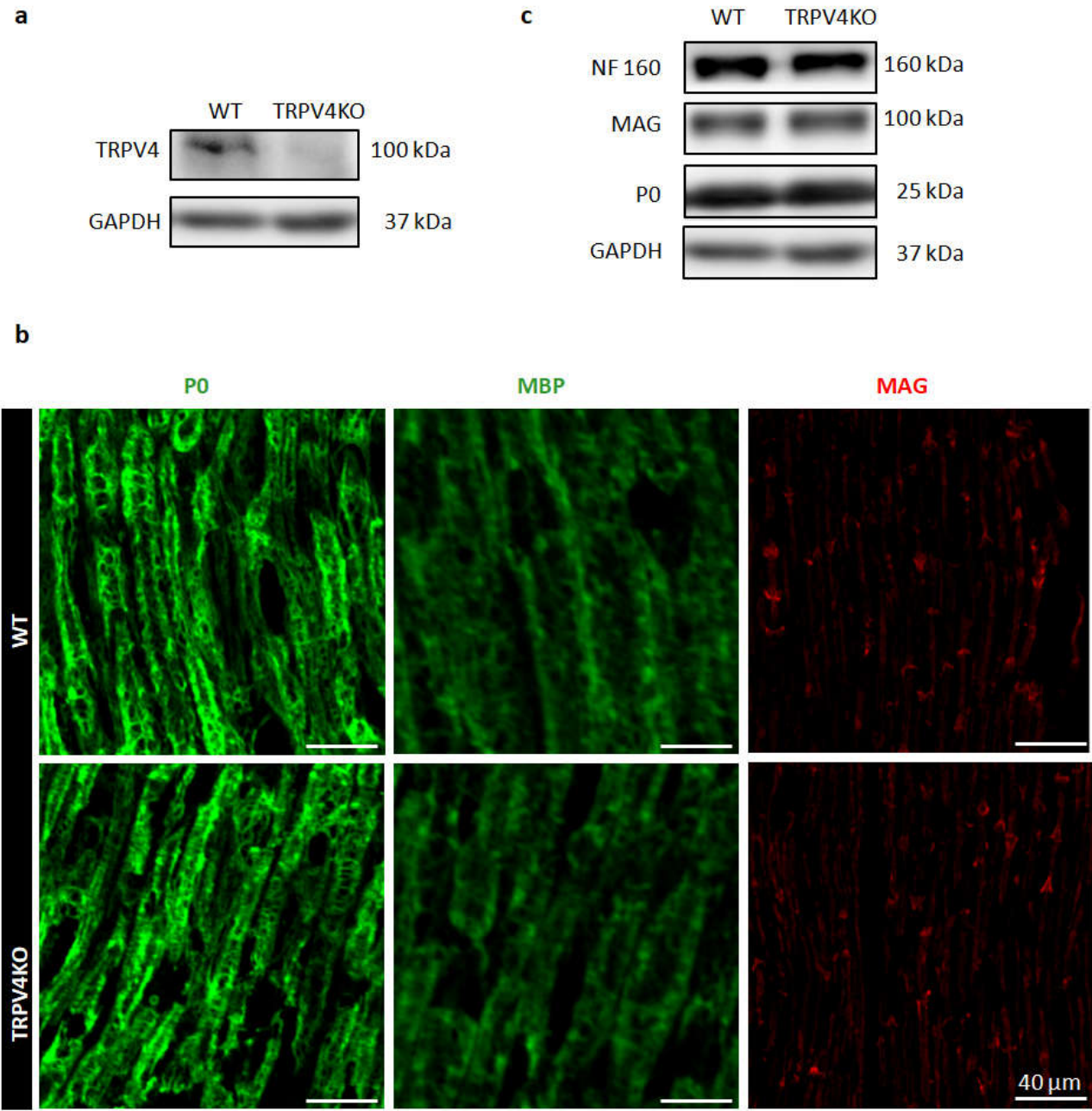


**Figure 5**

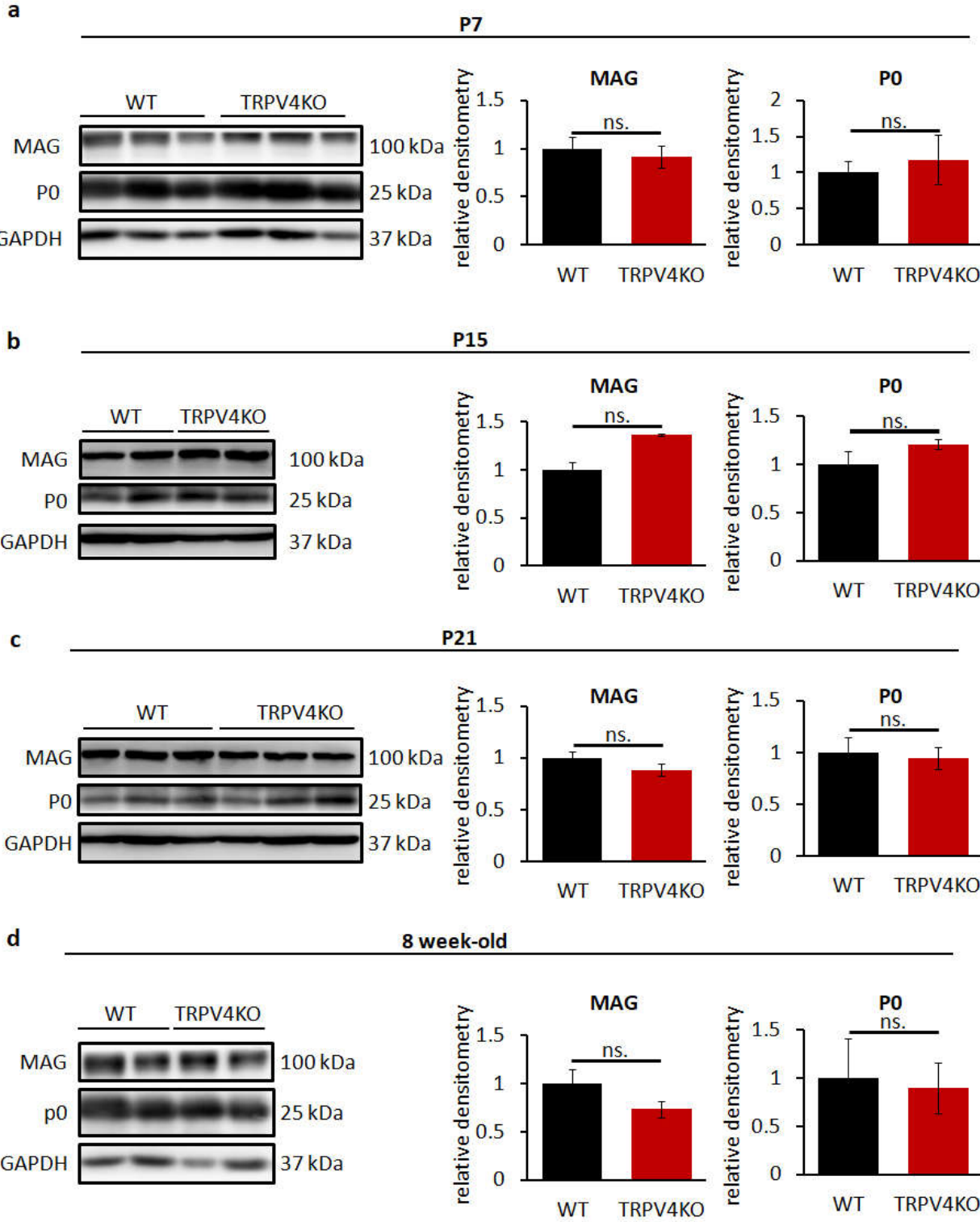


**Figure 6**

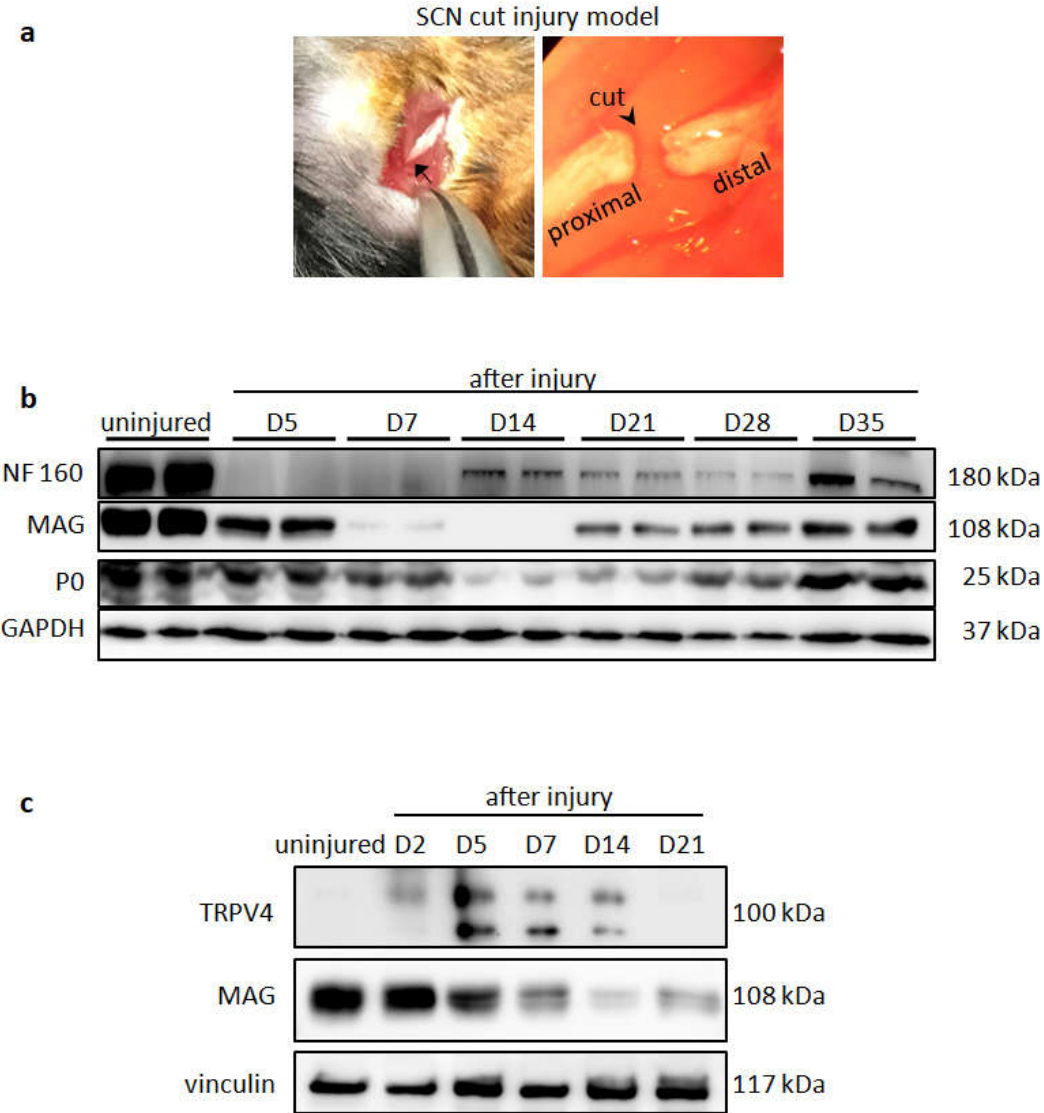


**Figure 7**

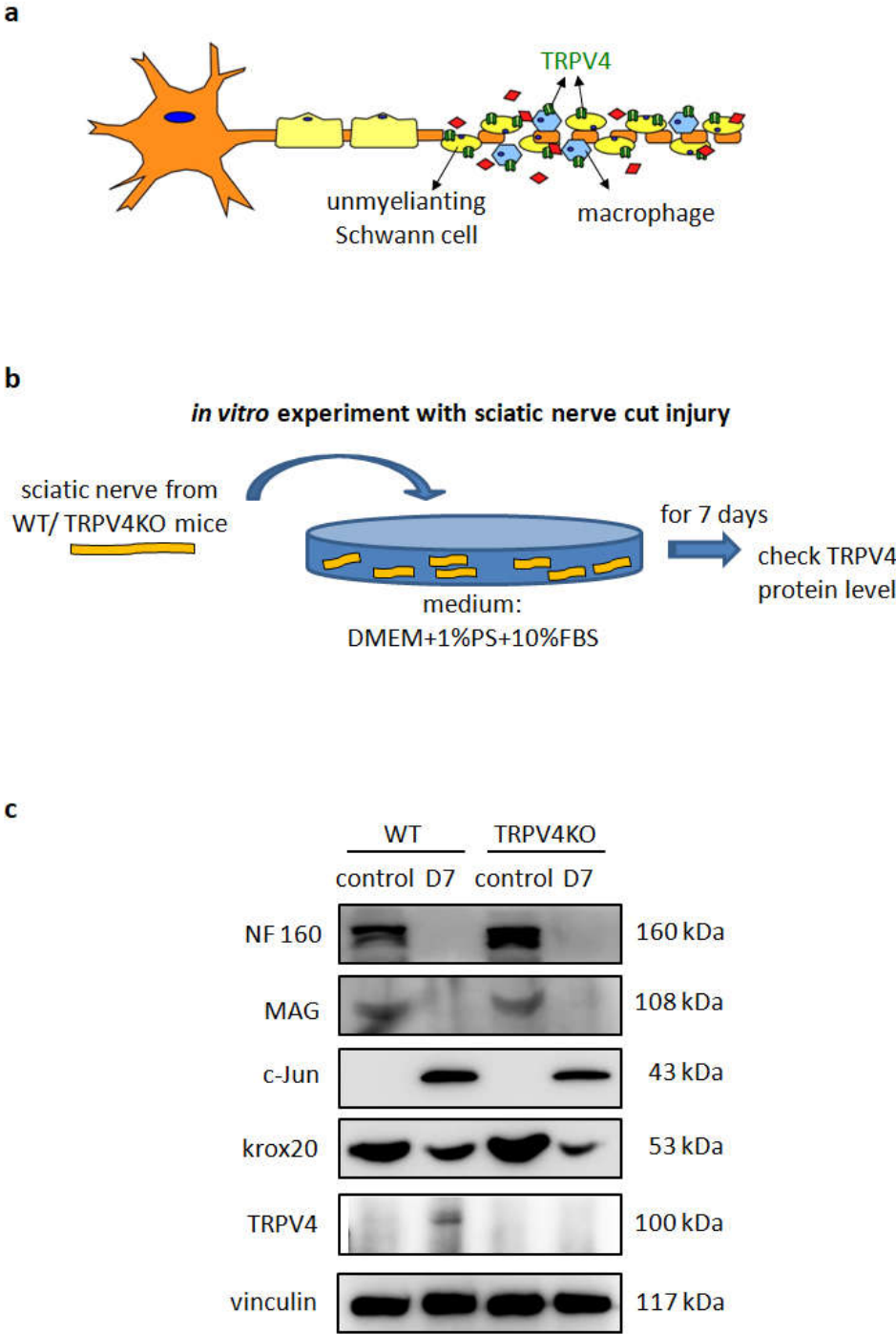


Figure 8

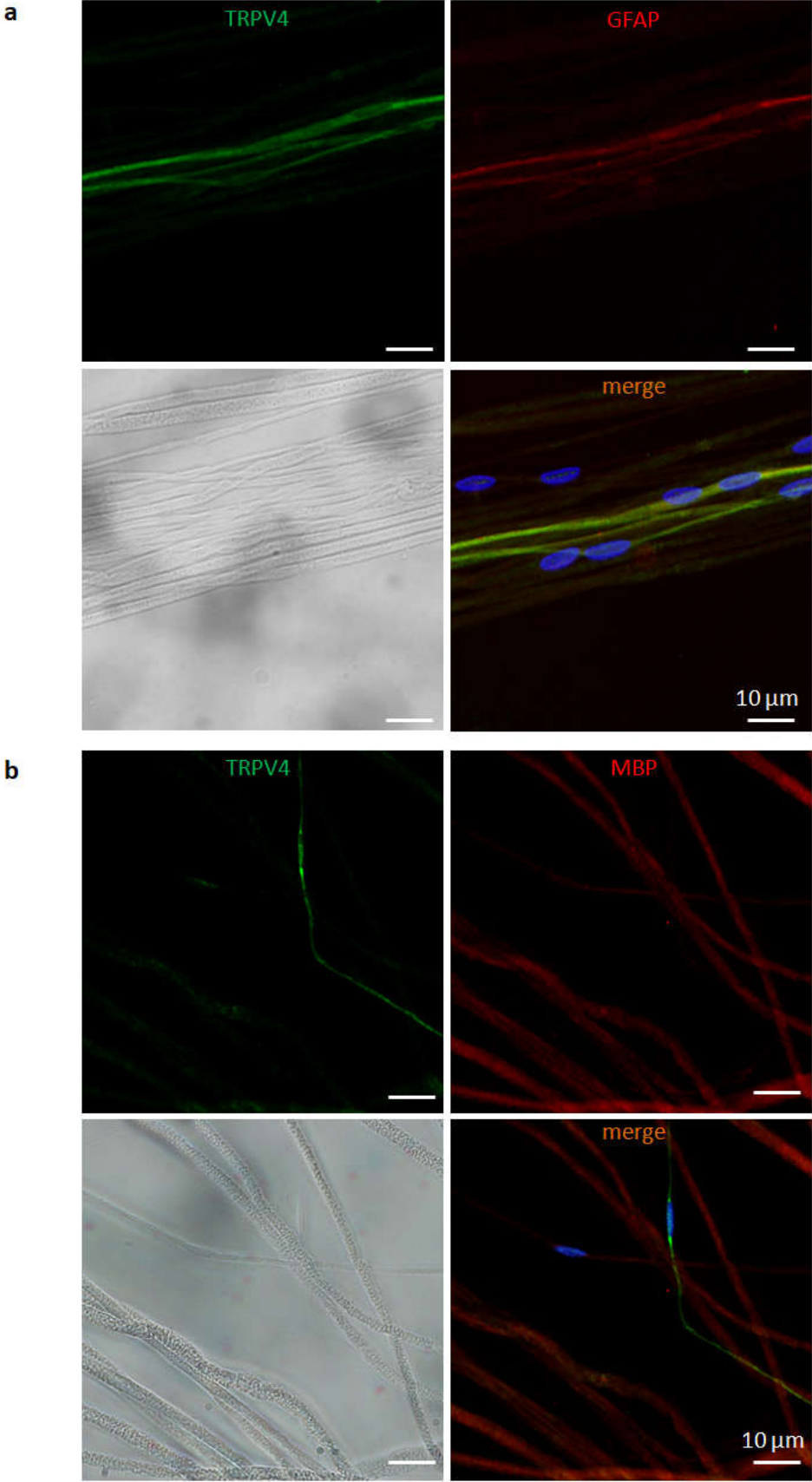


Figure 9

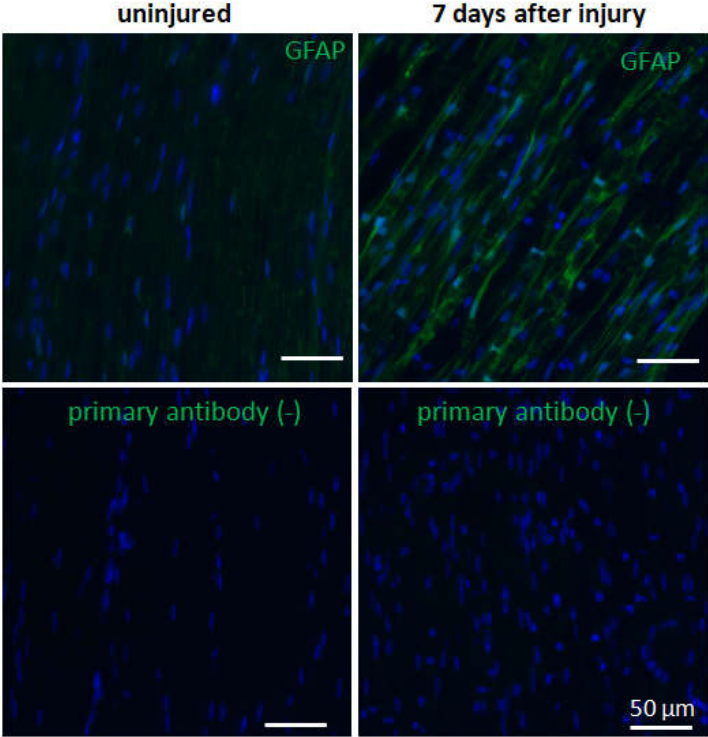
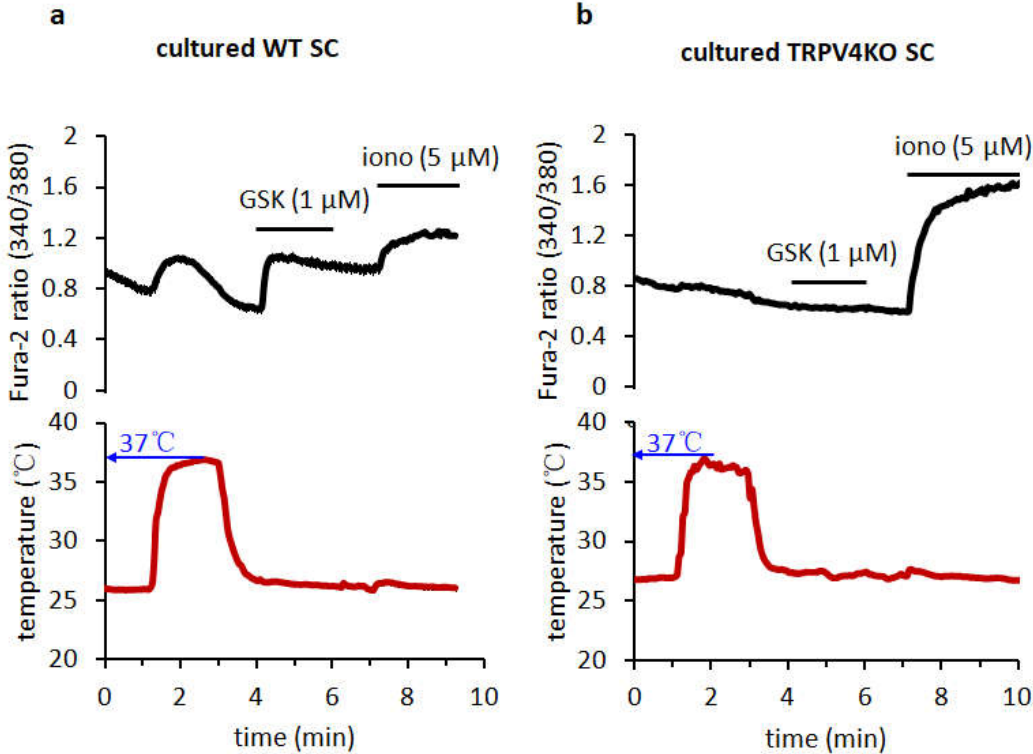


Figure 10



**Figure 11**

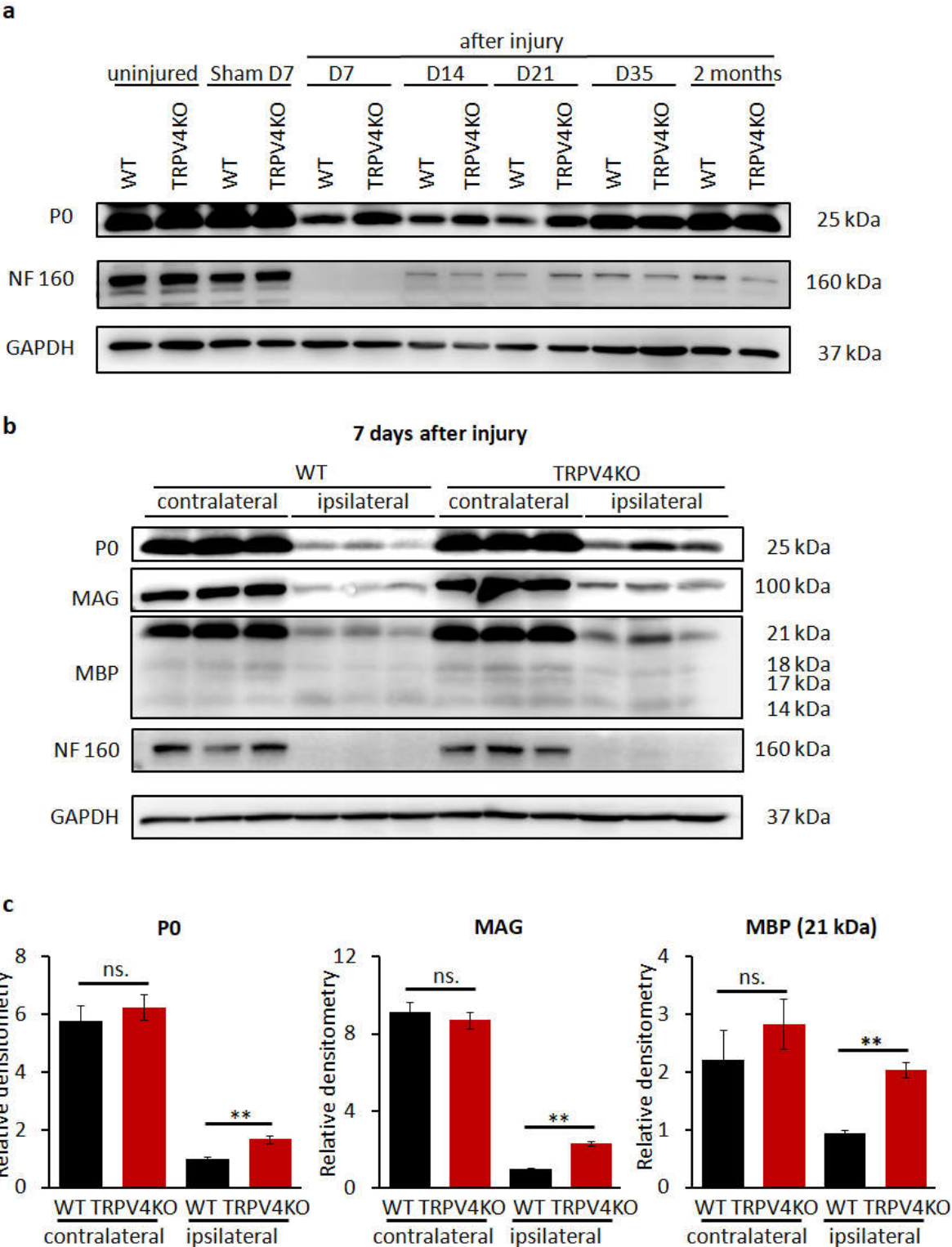


Figure 12

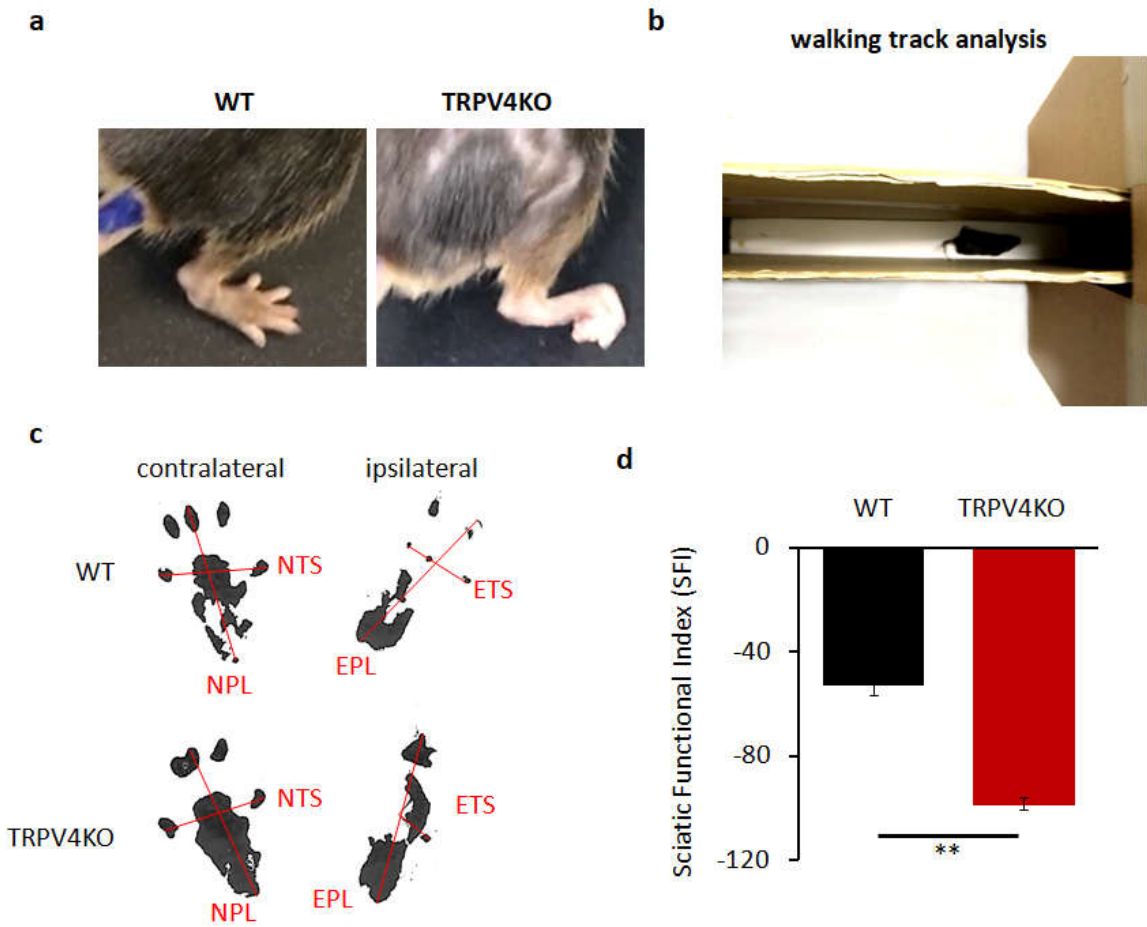
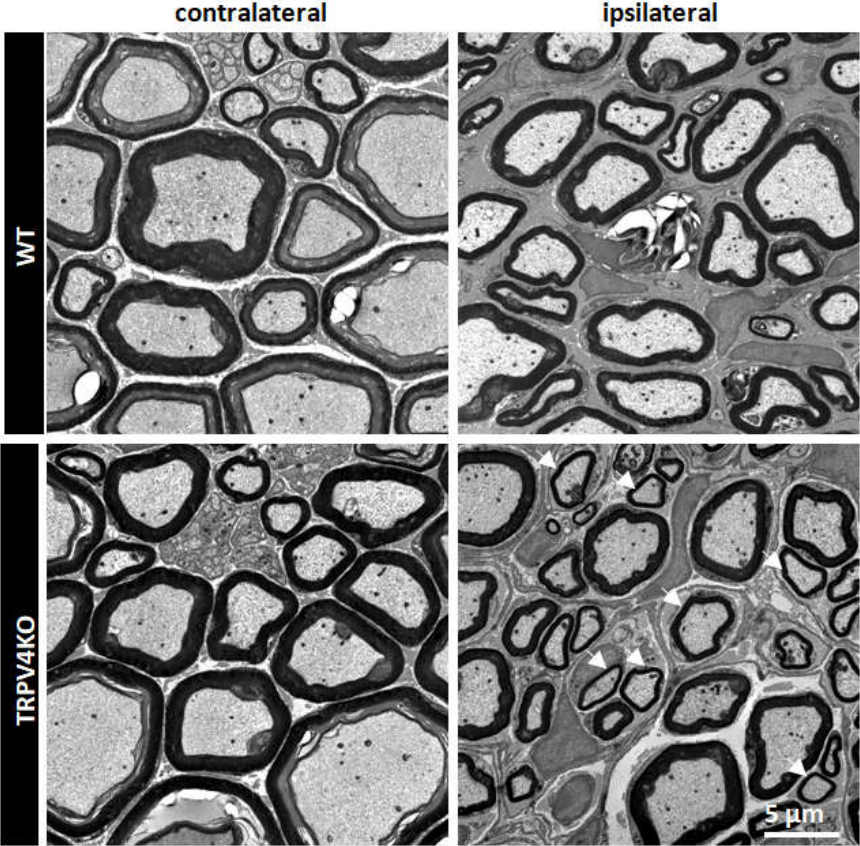
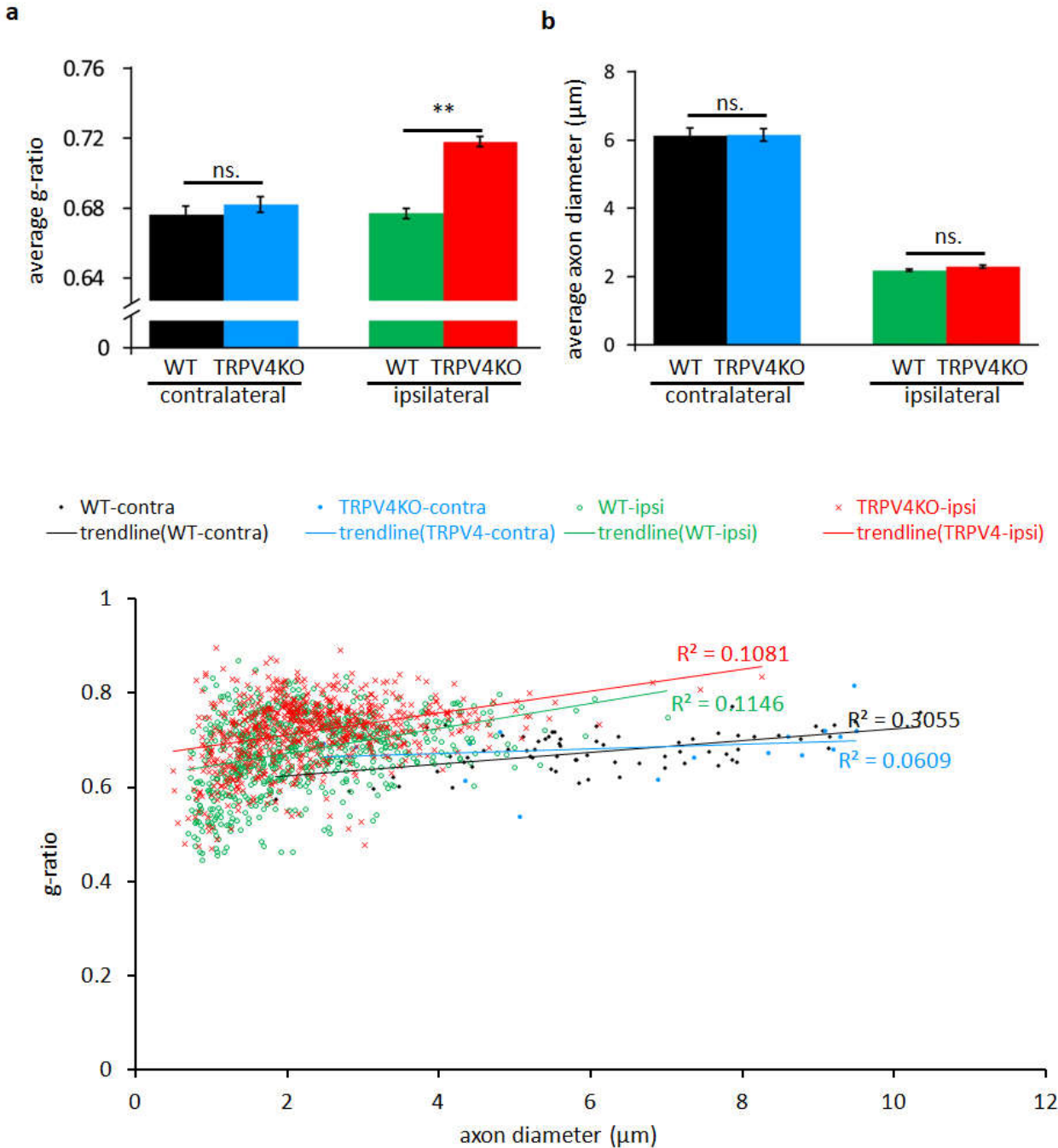


Figure 13



**Figure 14**



**Figure 15**

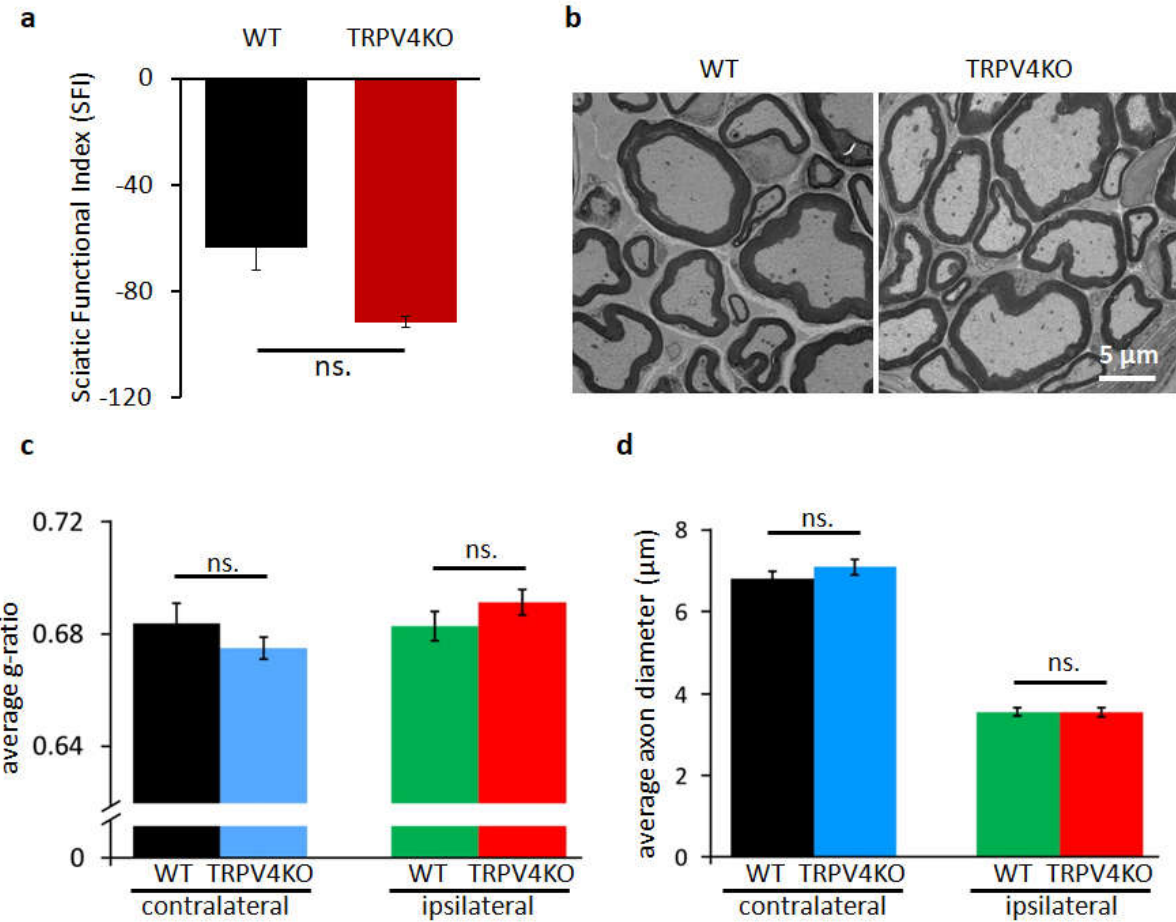
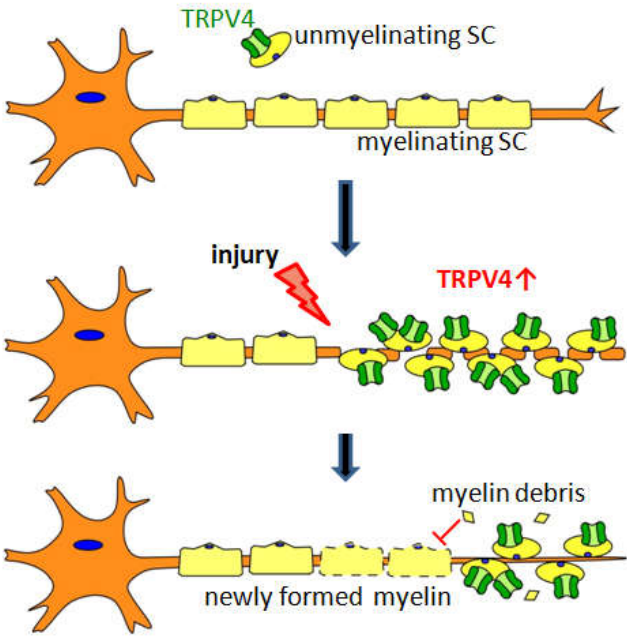


Figure 16



More amounts of myelin structure proteins could be remained in the injury site in TRPV4KO mice.

↓  
Recovery is delayed in TRPV4KO mice .